Zentralinstitut für Engineering, Elektronik und Analytik (ZEA), Systeme der Elektronik (ZEA-2)

Time-Independent Finite Element Simulations of Magnetic Behavior in an Actuator System Used for Research Concerned with Active Drag Reduction

Courtney Ford

Jül-4422

Mitglied der Helmholtz-Gemeinschaft

JÜLICH Forschungszentrum

Berichte des Forschungszentrums Jülich
Jül-4422 · ISSN 0944-2952
Zentralinstitut für Engineering, Elektronik und
Analytik (ZEA), Systeme der Elektronik (ZEA-2)

D 5 (Master Bonn, Univ., 2019)

Vollständig frei verfügbar über das Publikations-
portal des Forschungszentrums Jülich (JuSER)
unter www.fz-juelich.de/zb/openaccess

Forschungszentrum Jülich GmbH · 52425 Jülich
Zentralbibliothek, Verlag
Tel.: 02461 61-5220 · Fax: 02461 61-6103
zb-publikation@fz-juelich.de
www.fz-juelich.de/zb

Zentralinstitut für Engineering, Elektronik und Analytik (ZEA), Systeme der Elektronik (ZEA-2)

Time-Independent Finite Element Simulations of Magnetic Behavior in an Actuator System Used for Research Concerned with Active Drag Reduction

Courtney Ford

Supervisors/Gutachtern:

1. Gutachter: Prof. Dr. Ing. Stefan van Waasen (Forschungszentrum Jülich)
2. Gutachter: Dr. Dieter Eversheim (Universität Bonn)
Dr. Michael Schiek (Forschungszentrum Jülich)
Florian Seidler, M.Sc.(Forschungszentrum Jülich)

Abstract

Recent work in the field of drag reduction research has led to the realization that running transverse waves along the outer surfaces of aircraft and other motorized vehicles can lead to a reduction in the drag experienced by these vessels. To further investigate this phenomenon, actuators are needed that will create traveling transverse waves that behave according to the requirements for wind tunnel testing of small-scale models.

This Masters Thesis presents an investigation into the magnetic behavior of such an actuator, with a focus on modeling various magnetic configurations in order to optimize the Lorentz force experienced by coils in a stationary system. Using finite element analysis based simulation software, physical phenomena such as hysteresis are studied to determine the preferred magnet, coil, and metal configuration that will result in optimum actuator performance.

Contents

1 Introduction

One of the largest limiting factors in the efficiency of modern aviation is drag. As such, a great amount of research is currently being conducted for the improvement of aeronautics in the field of drag reduction. This thesis presents a work that contributed to the improvement of hardware used in testing new drag reduction methods in a wind tunnel.

1.1 FOR 1779

The research unit FOR 1779 is a collaboration between the Forschungszentrum Jülich and the Rheinisch-Westfälische Technische Hochschule (RWTH) in Aachen. Led by Prof. Dr. -Ing. Wolfgang Schröder, head of the aerodynamics department at RWTH Aachen, and using funding from the Deutsche Forschungsgemeinschaft (DFG), this unit is currently researching the reduction of turbulent drag on transport systems caused by surface oscillations and riblets (DFG, Li et al).

As this research unit is primarily concerned with wind tunnel testing, much of its effort goes into the development of technology to improve testing under these conditions. The actuator described in this thesis is specifically designed to optimize testing in a tunnel, while modern aircraft will probably use piezo-actuators to induce surface waves along the wings.

1.2 Biomimicry

Both transverse surface waves and riblets are ideas based on systems seen gracing the bodies of marine animals.

Transverse waves are derived from a feature exhibited in dolphin skin; when dolphins travel at high speeds, their skin produces small waves that travel over their bodies transverse to the direction of motion. Although more recent studies have shown that the effect of these waves on dolphins themselves is practically negligible, nevertheless the phenomenon has a large impact on artifically-produced objects, such as aircraft wings (Fish).

Likewise, riblets are derived from a feature exhibited on shark skin, which is covered in small, tooth-like scales called denticles. These denticles act as airfoils on the surface of the skin, both increasing lift (lateral lift in the case of

sharks) and decreasing drag (Wen et al).

1.3 Subproject 4

FOR 1779 is divided into five subprojects. Of these subprojects, it is the fourth, the aptly named 'Subproject 4,' with which this Master's thesis is concerned.

Supervised by Prof. Dr. Stefan van Waasen, institute director of the Electronic Systems section of the Zentralinstitut für Engineering, Elektronik und Analytik (ZEA-2) of the Forschungszentrum Jülich, this subproject is primarily concerned with the development of the hardware necessary to produce the transverse surface waves during FOR 1779's wind tunnel testing.

To accomplish this, Subproject 4 is tasked with the design, construction, and calibration of an actuation system that generates precise waves along a surface plate in a controlled fashion.

1.4 Purpose

The purpose of this Master's thesis is to conduct research regarding the magnetic behavior of the actuation system. It will focus on stationary studies, in particular comparing different configurations of magnets, metals, and coil geometries, in order to determine the optimum configuration to increase the Lorentz force generated on each actuator within the system. This research will be used to improve the system performance, and will be particularly useful for the design of a new actuation model.

In order to achieve this, simulations will be written and run using the program software COMSOL. These COMSOL simulations will be designed to measure both the magnetic flux at various positions between stacks of magnets and the Lorentz force acting on coils placed between them.

2 Background Physics

The pertinant electromagnetic interactions taking place within the actuation system can be described using three different concepts: Maxwell's equations, the Lorentz force, and the hysteresis of magnetic flux through metal.

2.1 Maxwell's Equations

Maxwell's equations are ubiquitous in electromagnetic research as they concisely describe the fundamental forces that result due to electricity and magnetism.

Originally containing twenty equations in 1879 when James Clerk Maxwell died abruptly from abdominal cancer, subsequent work by other physicists and further development of mathematical formulation reduced the number of Maxwell's equations to a mere four. These four equations are typically expressed as a series of either integral or differential expressions. The differential form is easier to use with finite element analysis, therefore the four equations shown in Table 1 are given in differential form (COMSOL, Bondeson et al).

$\nabla \cdot D = \rho$	Gauss' Law for Electricity
$\nabla \cdot B = 0$	Gauss' Law for Magnetism
$\nabla \times E = -\frac{\partial B}{\partial t}$	Faraday's Law
$\nabla \times H = \frac{\partial D}{\partial t} + J$	Maxwell-Ampère's Law

Table 1: Maxwell's Equations in Modern Form (Bondeson et al)

These are the equations used by the software program COMSOL to calculate magnetic flux in a simulation (COMSOL).

2.2 Force between Nearby Magnetized Surfaces

For the case in which two magnetized surfaces have been brought in close proximity to each other, the electromagnetic forces acting on the individual magnets can be derived using Maxwell's equations. When the air gap between the magnets is smaller than the magnets themselves, and ignoring fringe effects, the force between the surfaces can be found using the equation:

$$F = \frac{\mu_0 H^2 A}{2} = \frac{B^2 A}{2\mu_0} \tag{1}$$

Where F is the electromagnetic force between the magnets, μ_0 is the permeability of the material between the magnets, in this case air (with a value of $4\pi \cdot 10^{-7}$ Tm/A), H is the magnetic field, A is the area of each surface, and B is the magnetic flux density (Clarke, Humphries).

This equation is useful for determining the stability of magnets in their holders, in particular for comparing the magnitudes of the forces acting on individual magnets in different system configurations to ascertain which designs are more

stable.

2.3 Lorentz Force

Named after the Dutch physicist who first formulated it, the Lorentz force describes the force generated due to an electrical current moving in a magnetic field. In the absence of a free-standing electric field it behaves according to the equation:

$$\mathbf{F_L} = q\mathbf{v} \times \mathbf{B} = IN \cdot \mathbf{l} \times \mathbf{B} \tag{2}$$

Where $\mathbf{F_L}$ is the force on the current-containing coil, q is the charge of the particles in the current, $\mathbf{v}$ is the velocity of the particles in the current, $\mathbf{B}$ is the magnetic flux density, I is the current in the coil, N is the number of turns of the coil, and $\mathbf{l}$ is the length of the coil (Griffiths).

This force is perpendicular to both the current direction and magnetic field in the actuator, and the orientation of the force with respect to the current and field can be seen in the image in Figure 1.

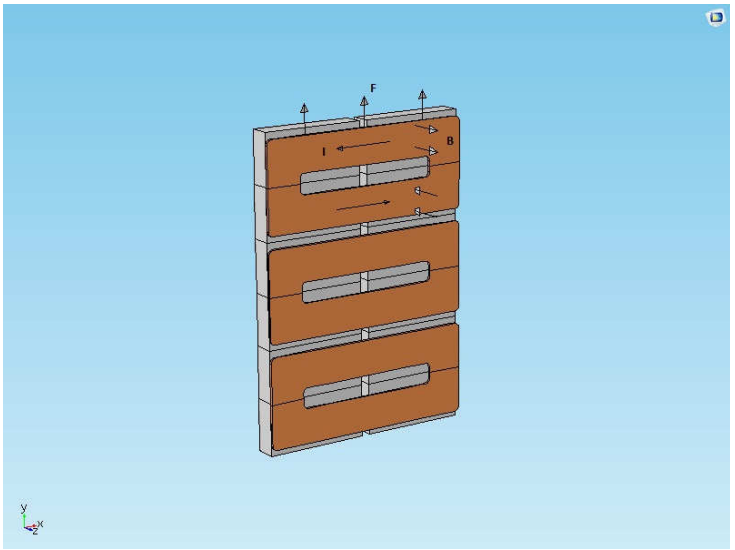

Figure 1: The Lorentz Force in Model 3.0

The rust-color represents the coils and the gray blocks represent the magnets

Image created using COMSOL

It is this force that is responsible for the movement in the actuator system.

2.4 Hysteresis

Hysteresis, which stems from the Greek word *hysteresis* meaning 'coming short' or 'a deficiency' which itself stems from the Greek word *hysteros* meaning 'later,' 'second,' or 'after' (Harper), refers to the lag in the change of a property of an object, in this case the magnetic flux density, compared to the external change of the same property (Britannica).

Specifically, when an external magnetic field is applied, the magnetic flux density through ferromagnetic material such as iron will not immediately change to match the external field, but will instead follow the path illustrated by a hysteresis curve (Britannica).

An example of a hysteresis curve used by COMSOL is shown in Figure 2.

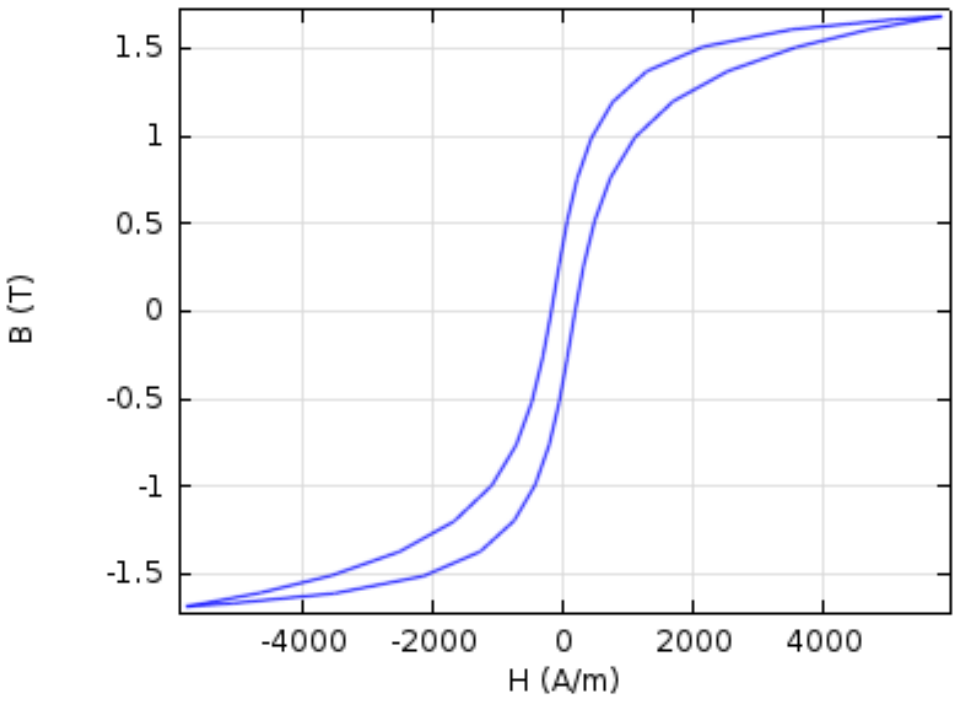

Figure 2: Example of a Steady-State Hysteresis Loop (COMSOL)

This graph plots the magnetic field density (B) through a material in Tesla against the external magetic field (H) in Amperes per meter. Depending on whether the external field is being applied or removed, the magnetic field density will follow the rightmost or leftmost curve respectively.

2.4.1 Methods of Applying Hysteresis to Stationary Systems

There are several different methods for applying hysteresis to time-independent systems. One of the most common is to replace the hysteresis curve with the average magnetic saturation curve (also known as the BH curve) of the material. Another well-known method is the Jiles-Atherton method.

2.4.1.1 Magnetic Saturation Curves

Within a small range of field values, magnetic flux density varies linearly with the application of an external magnetic field. However, outside of this range, a material will become saturated and begin approaching a limit in the amount of magnetic flux density it can hold. Graphs showing this initial linear rise/fall and eventual saturation are referred to as magnetic saturation curves (COMSOL).

The magnetic saturation curve of the hysteresis loop presented in Figure 2 is given in Figure 3.

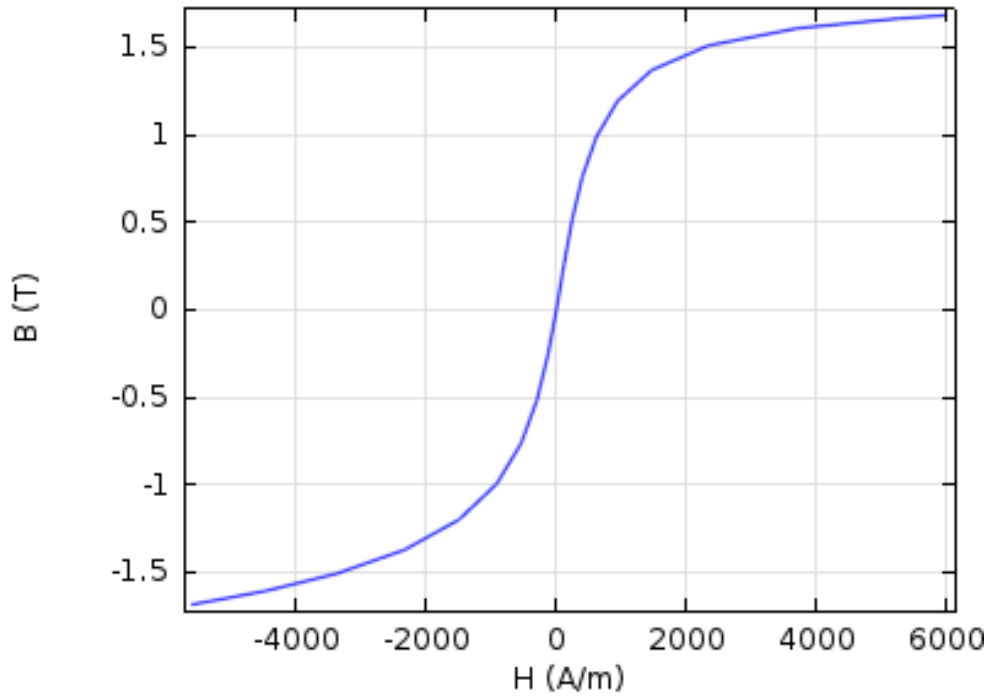

Figure 3: Example of a Magnetic Saturation Curve (COMSOL)

This graph averages the two time-dependent curves that compose the hysteresis loop, creating one time-independent curve that can be used regardless of whether the external magnetic field is being applied or removed (COMSOL).

Magnetic saturation curves are usually determined experimentally, and once found are typically employed in graphical form, rather than as equations. This can make them difficult to use in computer software programs, as enough data points must be entered into the computer to sufficiently represent the curve.

2.4.1.2 The Jiles-Atherton Method

The Jiles-Atherton method, however, takes a different approach. Developed in 1984 by D.C. Jiles and D.L. Atherton, in this method the hysteresis curve is defined by five parameters: saturation magnetization (M_s), Langevin slope (a), pinning coefficient (k), magnetization reversibility (c), and interdomain coupling (α) (COMSOL).

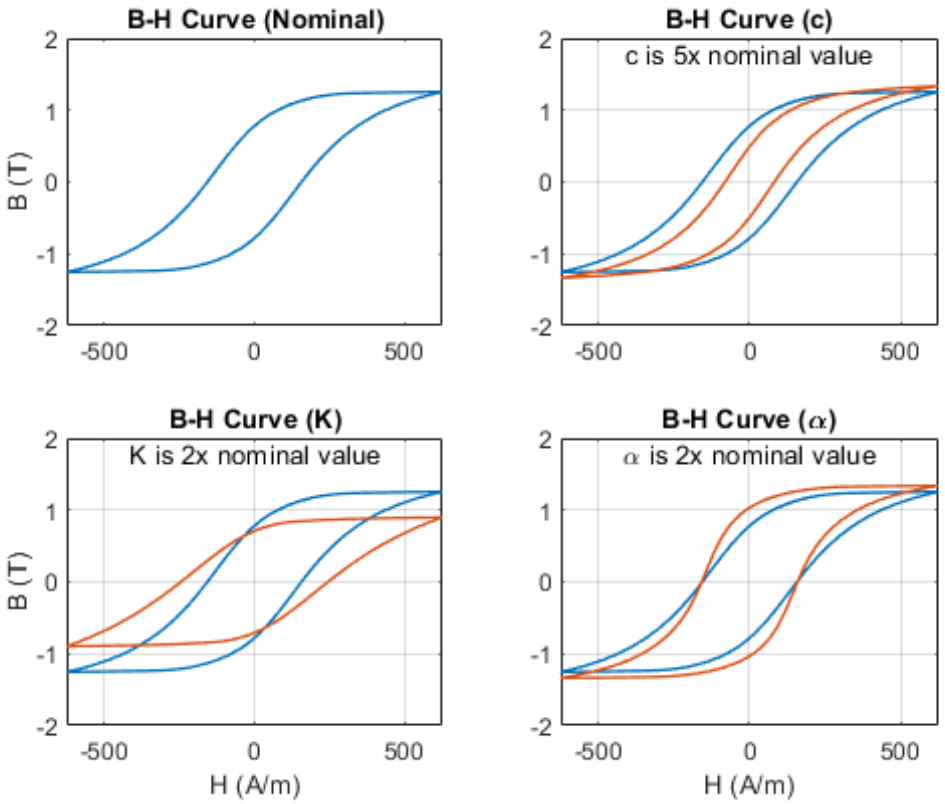

Figure 4: How the Jiles-Atherton Parameters Affect Hysteresis Curves (Mathworks)

Graphs depicting how three of these variables affect the hysteresis curve are given in Figure 4. In this image, the graph on the top left shows a hysteresis curve with baseline parametrization values (blue), while the other three graphs show both the baseline curve (blue) and a curve in which one of the parameters

has been changed (orange). The curve on the top right shows an altered c value, the curve on the bottom left shows an altered k value, and the curve on the bottom right shows an altered α value (Mathworks).

These graphs make it clear that the c value affects the gradient of the curve, the k value affects the intercepts along the H axis, and the α value affects the B axis intercepts (Mathworks). Additionally, the M_s value affects the maximum value of the B field while the a value affects the shape of the curve (Takacs).

Complex, time-independent hysteresis simulations often make use of Jiles Atherton models because the small number of variables leads to little memory usage by the simulations. However, the downside of using the Jiles-Atherton approach is that these models often experience convergence problems, especially in the determination of the correct value of the necessary variables.

3 Finite Element Analysis (FEA)

Finite element analysis was originally developed as a tool to approximate the solution to solid mechanics problems in the mid 1900s, but since then it has come to be used in many areas of physics and is particularly common in multiphysics analyses (COMSOL).

Mathematically, the behavior of physical systems is often expressed in terms of partial differential equations (PDEs). However, this presents a problem when it comes to analyzing the behavior of these systems, as most of these equations cannot be solved analytically. Instead, certain techniques exist that can be used to approximate the solutions to these problems. One of the most common techniques is finite element analysis (FEA) (COMSOL, Qi).

3.1 COMSOL

There are many software programs designed to use FEA to solve complex, interdisciplinary physics and engineering problems. The program used for this thesis is COMSOL.

COMSOL was founded in 1986 in Stockholm, Sweden by Svante Littmarck and Farhad Saeidi. Its primary product, COMSOL Multiphysics, was first released in 1998, and has since been expanded with a series of add-on modules in a variety of areas, including such diverse examples as AC/DC, Chemical Species

Transport, and Structural Mechanics (COMSOL).

The Multiphysics program includes solver and simulation software that uses finite element analysis to analyze coupled phenomena across multiple branches of physics. Additionally, it has been designed with a multitude of preset specifications in order to minimize the number of assumptions that must be made by the user (COMSOL).

The primary method used by COMSOL to model simulations is a version of finite element analysis known as the finite element method (FEM) (COMSOL).

3.2 Finite Element Method (FEM)

FEM involves reducing an object to a system of finite geometric shapes containing nodes (a practice known as discretization), and then using a series of equations acting within those finite elements in order to approximate a numerical solution to the partial differential equations acting on the entire object (COMSOL). Examples of these geometric shapes and nodes can be seen in Figures 5 and 6.

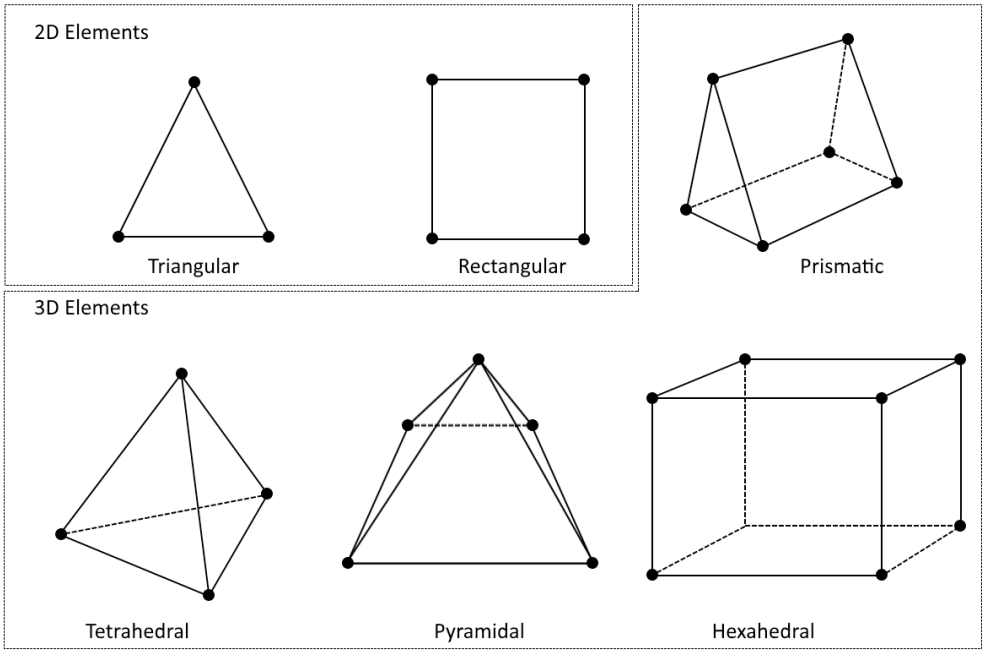

Figure 5: 2D and 3D Linear Elements Geometry and Node Placement (COMSOL)

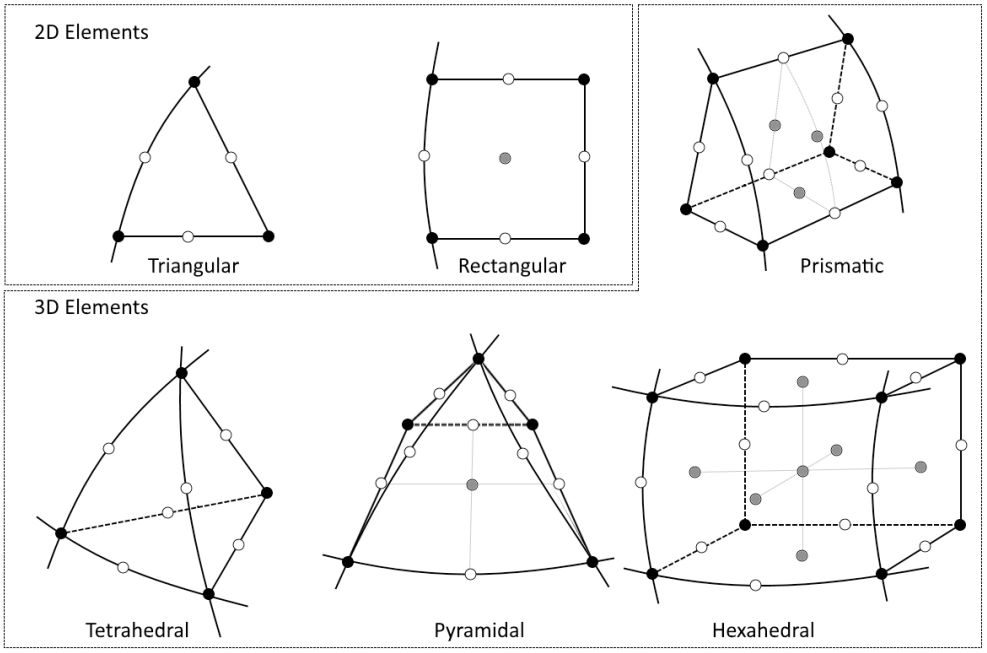

Figure 6: 2D and 3D Quadratic Elements Geometry and Node Placement (COMSOL)

The different colored nodes correspond to different element systems

3.2.1 Discretization

There are many different methods used for discretization, however they all have several features in common.

Discretization begins with dividing an object into a number of smaller elements. Next, equations are chosen to approximate the variation of the property in question (in this thesis usually the magnetic flux density) within each element. These equations are then solved, and in the case of integration over a domain the solutions are summed (Qi). An example of simple discretization over an integral is shown in Figure 7.

In this example, an integral over a specific range is discretized into $N = 1, 2, 4, 8$ elements. The value of the integral in each element is approximated using a constant function equal to the value of the function $y = x^2 + 6$ at the midpoint of the element. The integrals are calculated and for cases in which $N > 1$ they are summed to produce the total value of the approximation F. The approximated values are then compared with the calculated value for the example equation $\int_{-1}^{1} x^2 + 6dx \approx 12.667$ to find the error in the discretization approximation. As the figure shows, the higher the number of elements, the closer the value of the approximation to the calculated value (Qi).

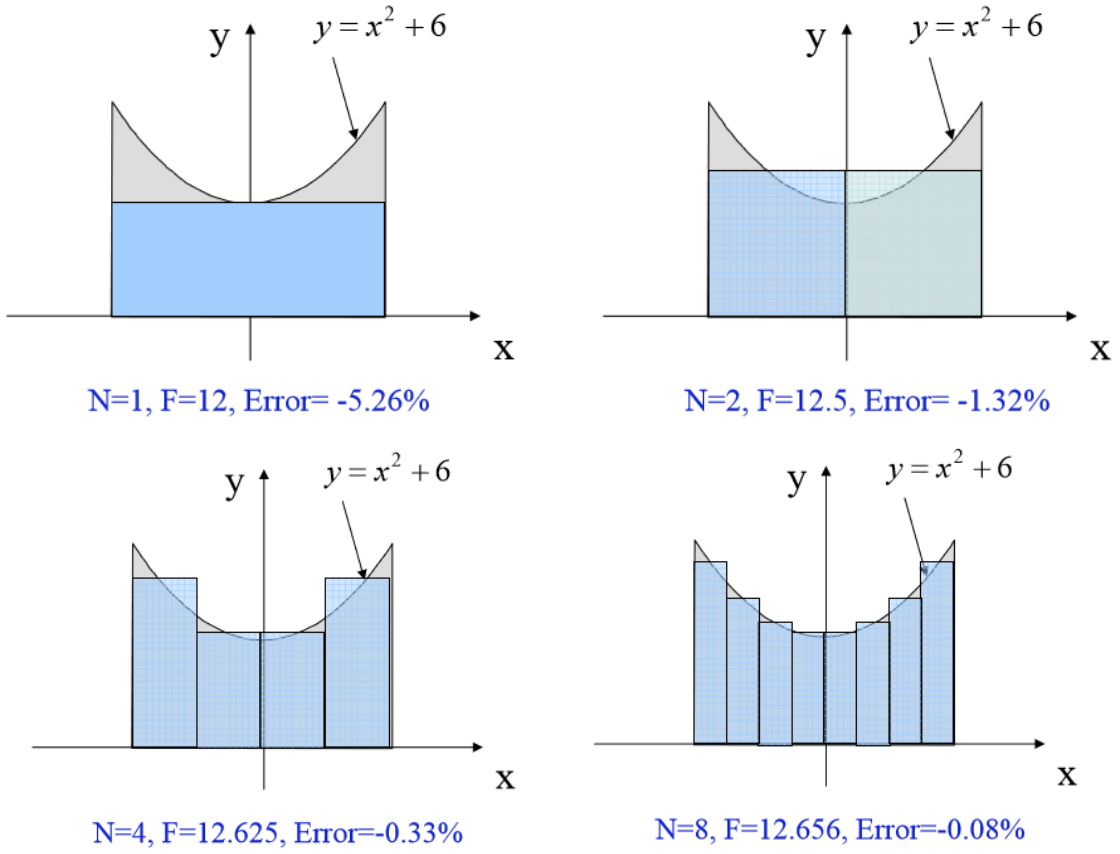

Figure 7: Example of Discretization with a Simple Function (Qi)

In COMSOL, discretization is accomplished by the use of the 'Meshing' node. This node has nine preset values, ranging from extremely coarse (discretization into a small number of large elements) to extremely fine (discretization into a large number of small elements), although it is not necessary to use the preset values and individual settings may be manipulated as desired. Furthermore, the user may choose between using several different shapes for the elements (such as free tetrahedrals or quads), and the shapes and sizes of the mesh of individual parts can vary within a simulation.

A higher number of elements always corresponds to a smaller relative error but also a longer runtime, and a balance must be found between the two to ensure accurate results within a reasonable timeframe. Additionally, different mesh shapes will result in higher or lower error values depending on the geometry of the model, although COMSOL uses free tetrahedrals as the default shape as this will usually produce more accurate results.

3.2.2 Element Order, Shape, and Nodes

The element shape and node options for two dimensional and three dimenstional simulations are shown in Figures 5 and 6 for linear and quadratic discretization geometries respectively. For the linear geometries the surfaces and edges are always flat, straight lines, however for the quadratic geometries the edges and surfaces of elements facing external domain boundaries are typically curved, while the edges and surfaces of elements facing the inside of a domain are typically straight or flat (COMSOL).

4 The Actuator

Producing the transverse surface waves for study in a wind tunnel requires the use of an actuator.

There have been three actuator designs thus far: Models 1, 2, and 3.

4.1 Model 1.0

The first model produced by Subproject 4 could produce a running wave with a minimum wavelength of 160 mm, amplitudes between 50 μm and 500 μm, and run at frequencies of up to 81 Hz.

Model 1.0 contained ten actuators, composed of copper coils made with a wire wound for 200 turns and separated by a distance of 20 mm. These coils were glued onto a glass-fiber reinforced plastic (GRP) board which was specifically designed with indentations to accommodate the coils and cutouts to reduce the weight of the actuators. An example of one of these coils glued to a GRP board can be seen in Figure 8.

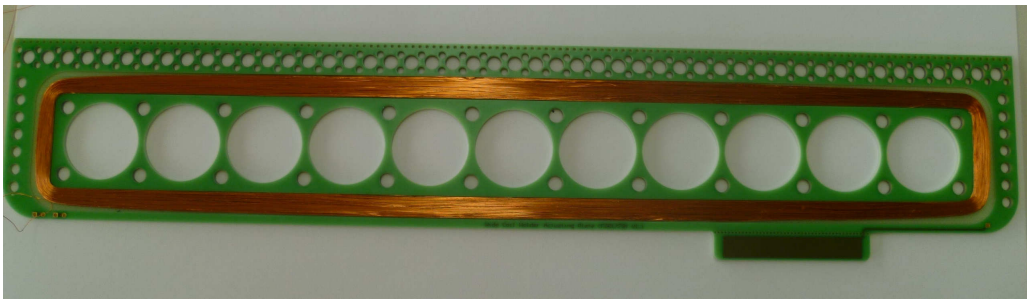

Figure 8: Coil Mounted on GRP Board for Model 1.0

At evenly-spaced intervals between and outside of the coils were sets of eight magnets arranged in two rows. The magnetic poles of the different rows were oriented in opposite directions, as can be seen in the side view diagram shown in Figure 9.

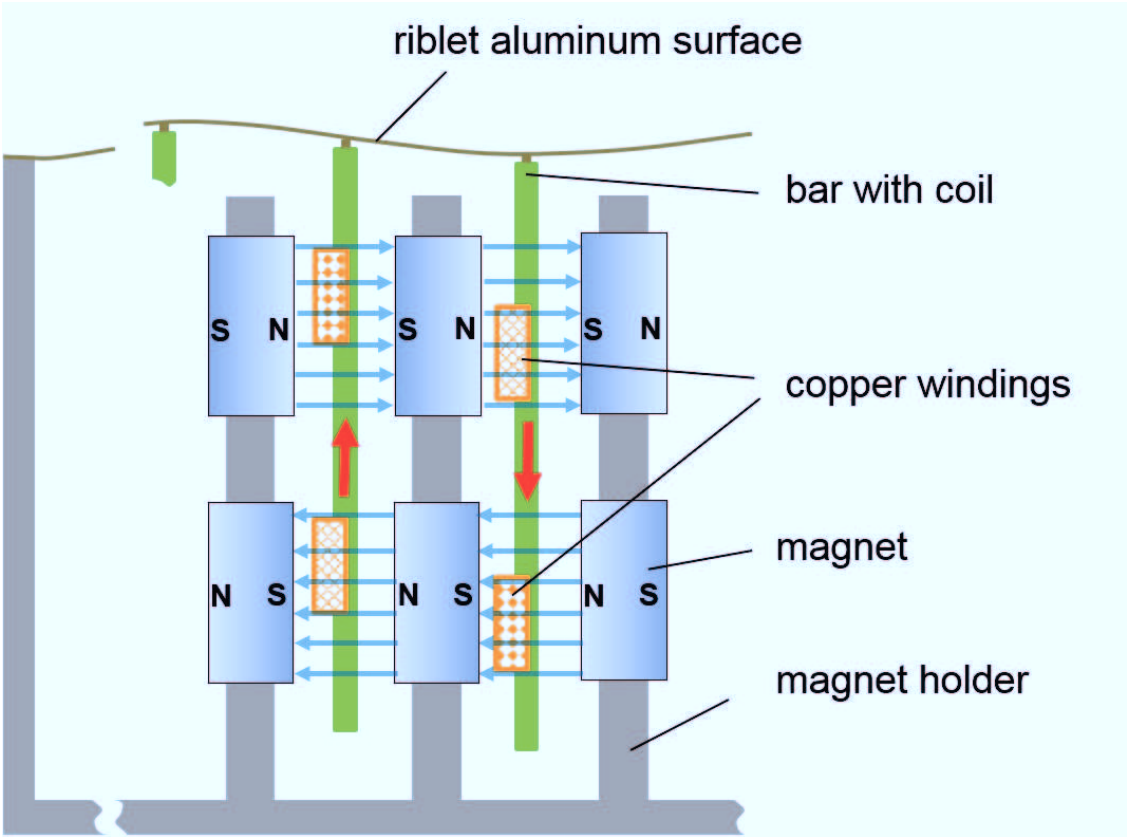

Figure 9: Sideview of Model 1.0 and Model 2.0

An internal view of the partly constructed Model 1.0 can be seen in Figure 10.

4.2 Model 2.0

Work on this Master's thesis began when Model 2.0 was the current actuating system. Model 2.0 could produce waves with a minimum wavelength of 80 mm, an amplitude of 260 to 500 μm, and at frequencies from 81 Hz to 135 Hz.

Model 2.0 contained twenty actuators, composed of copper coils made with a wire of diameter 0.27 mm wound for 80 turns. These coils were also glued onto GRP boards which were specifically designed to keep the weight low. An example of a GRP board without the coil can be seen in Figure 11.

Figure 10: Internal View of Model 1.0

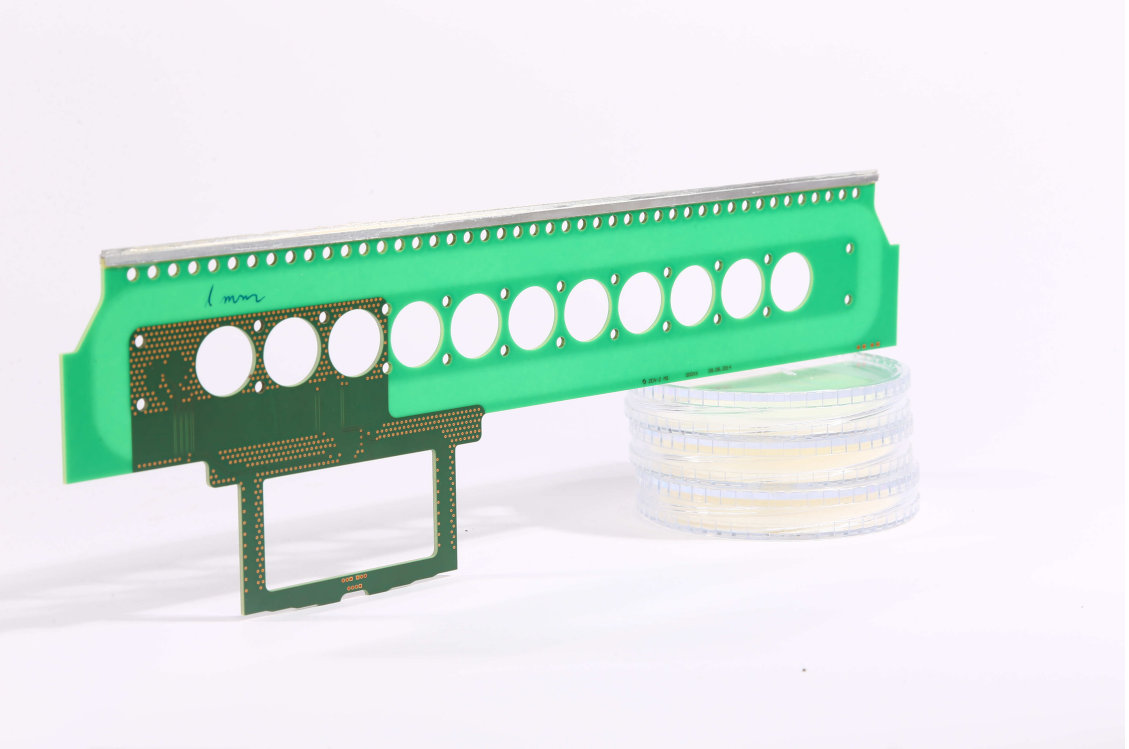

Figure 11: GRP Board for Model 2.0

The GRP boards had small aluminum plates glued to the top in order to increase the contact area between the boards and the surface. A close-up view of the aluminum plates can be seen in Figure 12.

Like Model 1.0, two rows of magnets with their poles arranged according to the diagram in Figure 9 were placed between and outside of all of the coils. These neodymium N48 magnets were held in place by twenty-one aluminum magnet

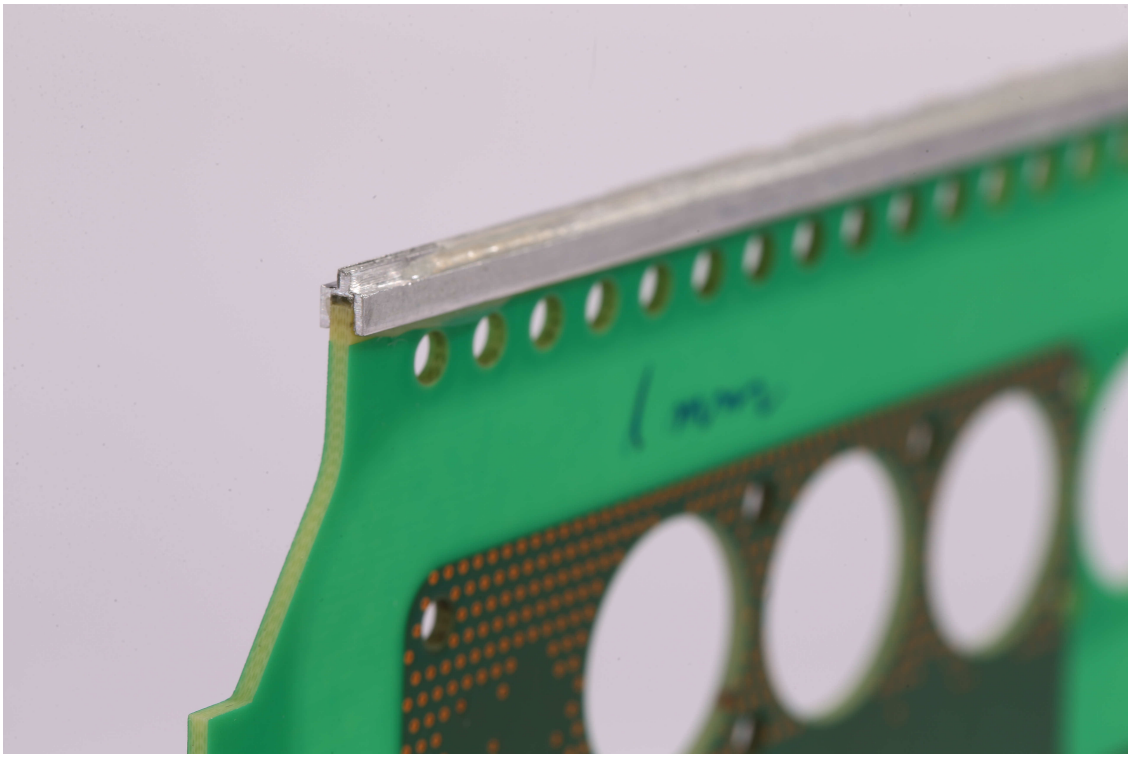

Figure 12: Al Plate Glued to the Top of a GRP Board

holders. While all of the magnets had the same width and height dimensions (50 mm x 15 mm) there were two different magnet depths: the magnets between the actuators had a depth of 5 mm while the magnets outside of the actuators were slightly larger with a depth of 15 mm.

Larger magnets were chosen for the outer magnet holders in order to compensate for the lower magnetic field that would be felt by coils on the far ends of the system that had less influence from nearby magnets as coils in the middle of the system. However, these larger magnets actually increased the field at the edges so much that the outer coils experienced slightly larger Lorentz forces than the coils near the center of the system.

The full system can be seen in Figure 13.

4.3 Model 3.0

A few months after I joined the project, planning began for Model 3.0. This model was designed to produce waves with a minimum wavelength of 80 mm, a maximum amplitude of 1 mm at a frequency of 81 Hz to 135 Hz, and a maximum amplitude of .5 mm for frequencies between 135 and 200 Hz.

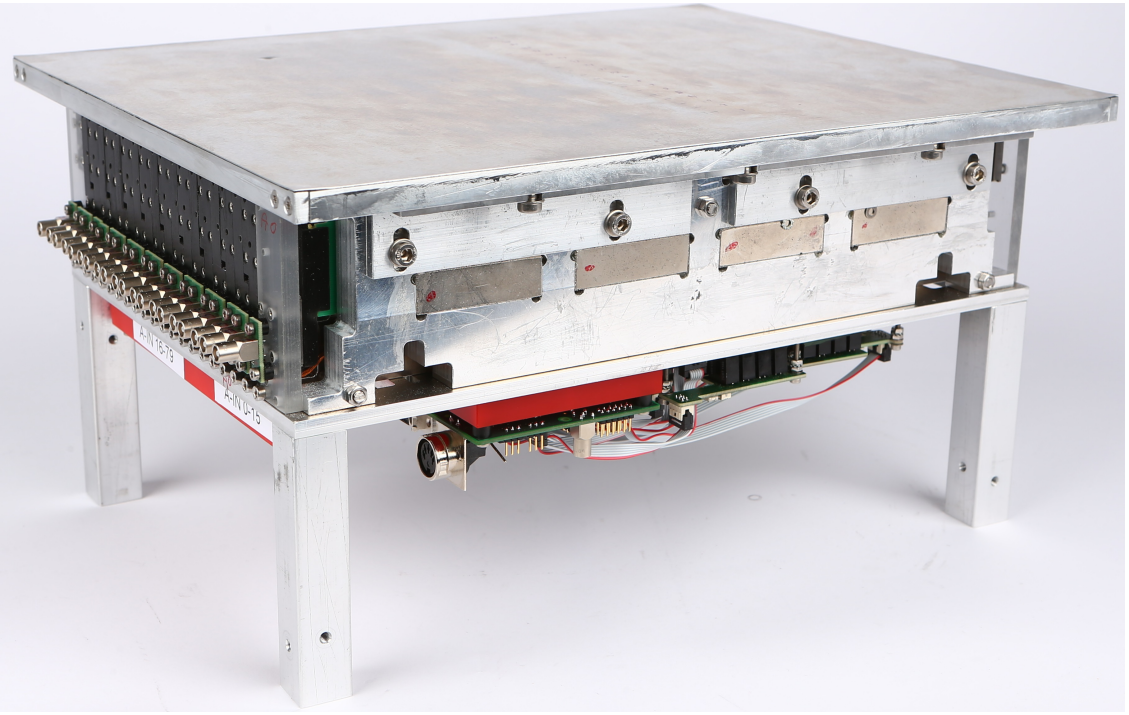

Figure 13: Model 2.0

The design of Model 3.0 was a slight departure from the earlier two models - a result of the research that had been conducted in the intervening time. Model 3.0 contained fifteen actuators, composed of six copper coils each (for a total of 90 coils for the full system) with a wire of diameter 0.355 mm wound for 140 turns. Like Models 1.0 and 2.0, these coils were glued onto a GRP board with a custom design to hold the coils in place and to reduce weight.

Similarly to Models 1.0 and 2.0, Model 3.0 also alternated actuators and groups of magnets. However, unlike the earlier two models, Model 3.0 did not have groups of eight magnets in two rows, but instead groups of twenty-four magnets in four columns. An example of the magnet and coil configuration in Model 3.0 is shown in Figure 14.

Additionally, unlike Model 2.0, Model 3.0 did not have larger magnets outside of the actuators. Instead, all of the magnets in Model 3.0, both between the actuators and outside of the system, had the same depth. A different method was used to compensate for lower magnetic fields near the edges of the system: u-shaped steel blocks. These blocks were added to the outside of the outer magnets in order to enhance the magnetic field affecting the outer actuators. Two pictures showing these steel blocks attached to a reduced, three-actuator system are included in Figure 15.

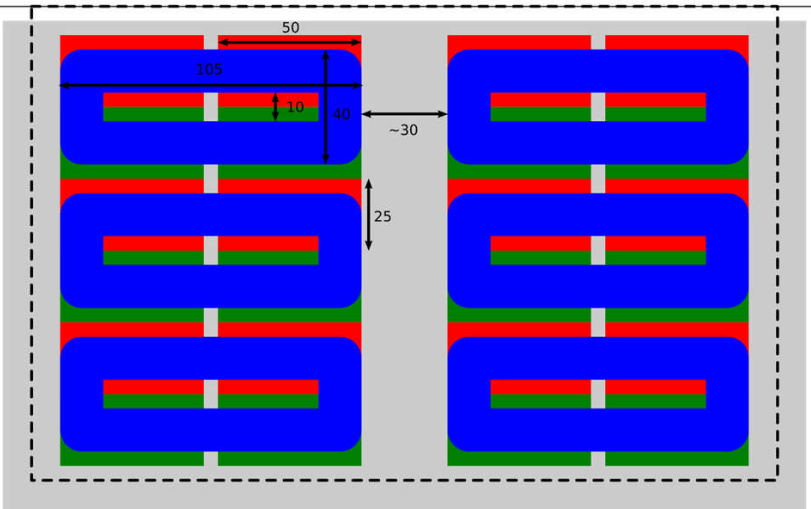

Figure 14: Magnet and Coil Arrangement in Model 3.0

The coils are in blue while the green and red represent magnets with opposite orientations. All dimensions are given in mm.

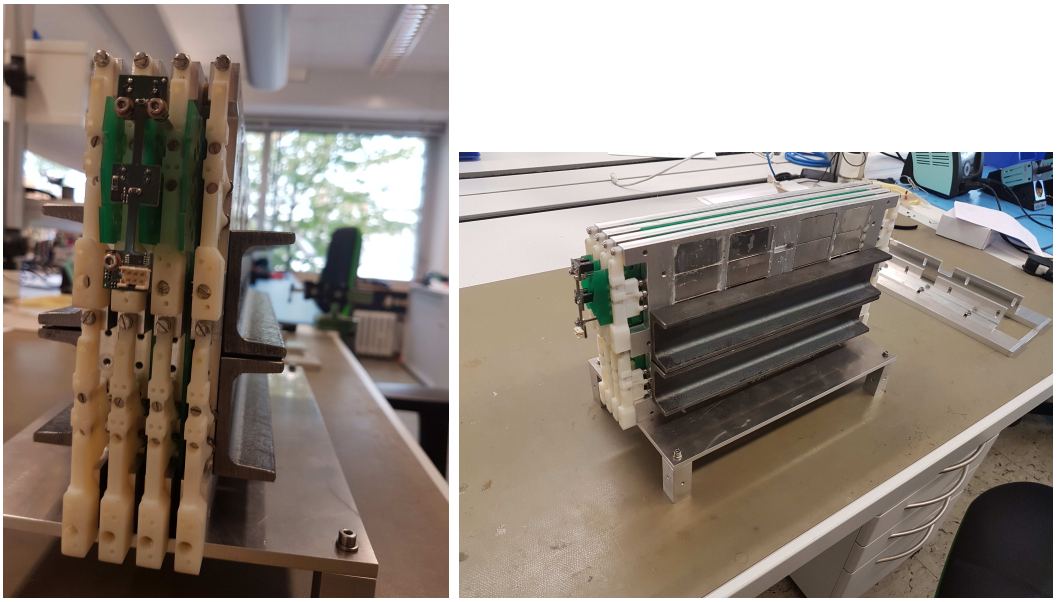

Figure 15: Steel Blocks on Reduced Model 3.0

Side and front views

4.4 Materials

There are five basic materials that are included in the actuator, with a sixth material (air) that merits consideration in the system. COMSOL contains all of

the necessary preset data for most of these materials, the two exceptions being the material used for the magnets (N48) and soft iron.

Table 2 displays the pertinant material information included in the COMSOL program.

Material	Electrical Conductivity (S/m)	Rel Permeability	Rel Permittivity
Air	0	1	1
Aluminum (Al)	3.774×10^7	1	1
Copper (Cu)	5.998×10^7	1	1
Circuit Board (FR4)	.004	1	4.5
Neodymium (N48)	0.667×10^6	1.05	1
Soft Iron (Fe)	4.032×10^6	1000	1
Steel SR235	1.12×10^7	1500	1

Table 2: Material Properties for Selected Materials

Highlighted values were not included in the COMSOL preset materials and had to be found from other sources (COMSOL, NPL, Ambrosio et al).

4.4.1 Neodymium Magnets N48

Neodymium magnets are composed of an alloy that combines neodymium, iron, and boron according to the formula $Nd_2Fe_{14}B$. Both General Motors and Sumitomo Metals developed these magnets independently in the 1980s as part of projects to find a replacement for expensive Sm/Co magnets, which were the common magnets of the time. They have the highest remanent magnetic field of any material currently commercially available for permanent magnets (Lucas).

The classification N48 is derived from the main element in the magnets (N for neodymium) and from the energy stored in the remanent magnetic field (48 MGOe).

5 Basic Measurements

Basic measurement simulations were simplistic systems designed to verify that the results generated from the simulation software were consistent with results garnered from hand calculations of similar situations. They were also helpful for testing the behavior of COMSOL under a variety of input parameters, as well as diagnosing problems when simulations of more complex systems returned

unexpected results.

The geometries of these systems consisted of simple parts, with each one containing only three domains (including an air sphere). Throughout the course of this thesis three simple simulations were designed: force on a coil by a c-shaped magnet, force between two block magnets, and hysteresis of metal inside a c-shaped magnet.

5.1 Force on a Coil Caused by a Classic C-Shaped Magnet

The first basic simulation designed for this project was created to verify that a magnet surrounding one small section of a large coil would only produce magnetic flux through the coil section surrounded by the magnet. Additionally, this simulation was created to confirm that such a model would produce a Lorentz force at right angles to both the magnetic flux and the current moving through the coil.

Geometrically, this program was simple: a c-shaped magnet was modeled, and a coil was run through the gap between the magnet poles. Surrounding both of these was a sphere of air.[1] An image of the simulation geometry is included in Figure 16.

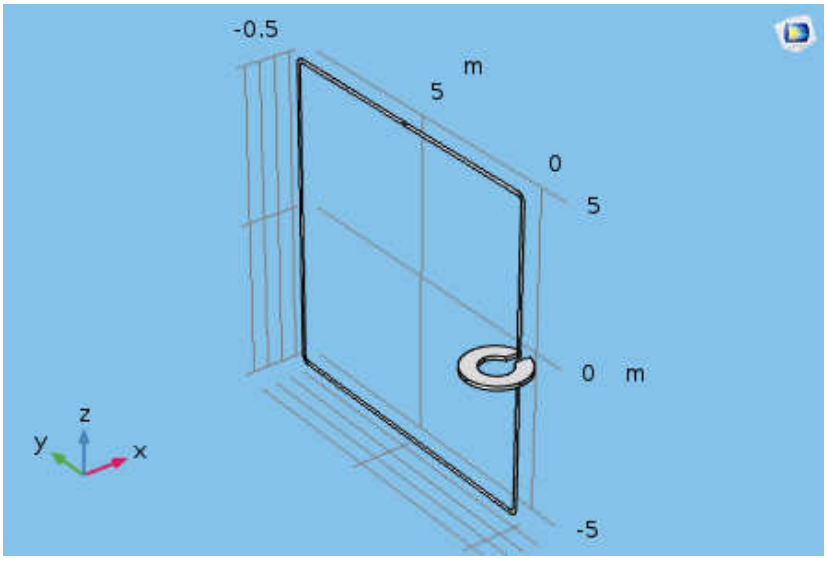

Figure 16: C-Shaped Magnet with Coil

Image created using COMSOL

[1] although all simulations include an air sphere or cube, for simplicity this domain is often excluded from images and geometric descriptions

As expected, magnetic flux density was only found in relevant quantities in the magnet and the gap between the magnet poles. This can be seen in the images in Figure 17, which include a zoomed out view of the entire coil and magnet, as well as two zoomed in views: one centered on the magnet and the coil running through it and the other the same view with the magnet removed to better show the distribution of flux density running through the coil.

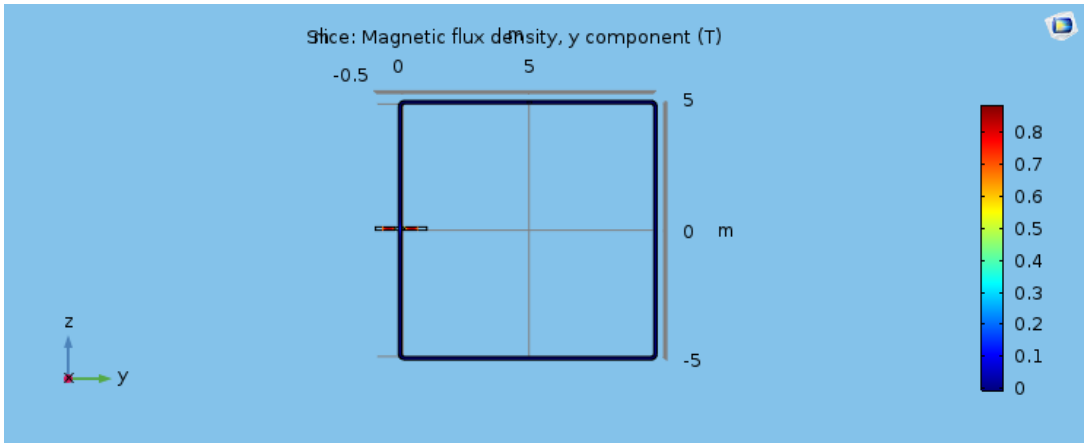

(a) Zoomed Out

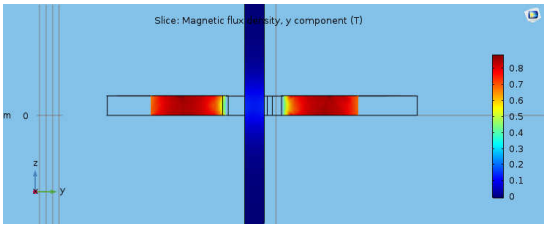

(b) Zoomed in with Magnet

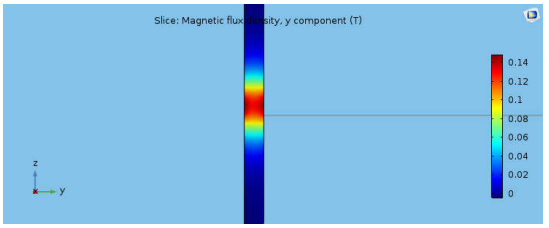

(c) Zoomed in without Magnet

Figure 17: Magnetic Flux through the Coil and Magnet in the Y Direction

Images created using COMSOL

The Lorentz force also behaved as anticipated, with non-negligible quantities only occuring in the section of the coil passing between, slightly above, and slightly below the magnet poles. Figure 18 depicts the Lorentz force in this simulation, including a zoomed out view showing the coil and magnet in their entirety, as well as a view zoomed in on the area of interest between the magnet poles.

COMSOL measured the value of the Lorentz force through the coil to be 0.349 N. This is very close to the 0.35 N force found by using Equation 2 given in Section 2.3 with the values used the in simulation.[2]

[2] $I = 1A$, $N = 10$, $l = 0.125m$ (the value of the length of coil over which the magnetic flux was greater than half of its maximum value in the coil (approximately twice the length over which the magnets were positioned)), and the maximum value of the magnetic flux through the coil $B = 0.14T$

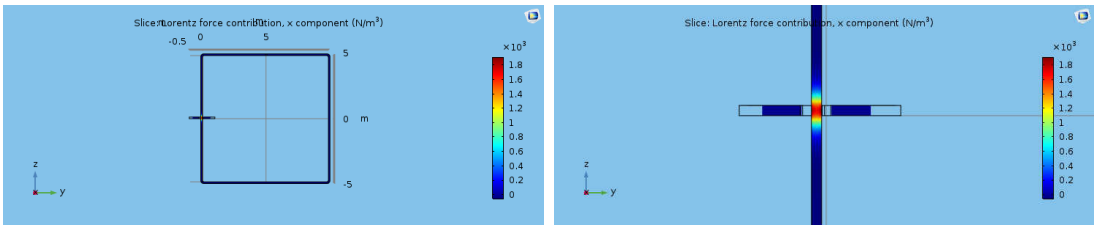

(a) Zoomed Out (b) Zoomed in with Magnet

Figure 18: Lorentz Force through the Coil and Magnet in X Direction

Images created using COMSOL

5.2 Force between Two Magnets

The second basic simulation created for this project was designed to test how COMSOL calculates forces on multiple objects. In this simulation, two magnets of opposite polarity were placed next to each other as shown in Figure 19.

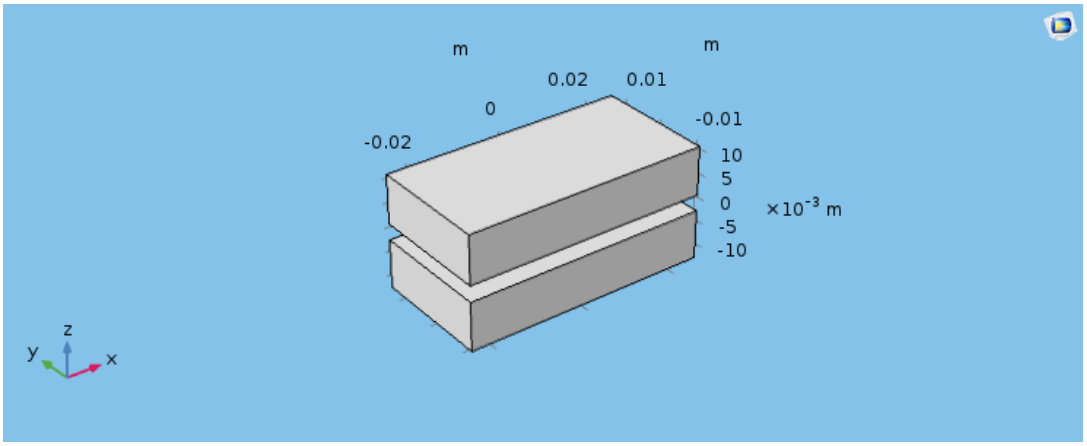

(a) Pair of Magnets of Opposite Polarity

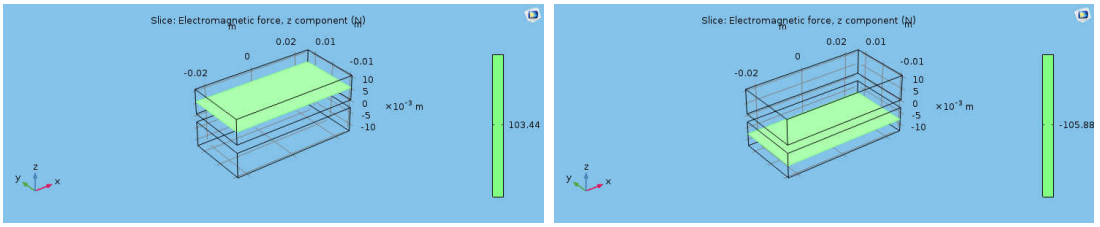

(b) Total Forces on Top Magnet (c) Total Forces on Bottom Magnet

Figure 19: Forces on a Pair of Magnets of Opposite Polarity

Image created using COMSOL

Force calculations were performed on each magnet, individually measuring the sum of all forces acting on them. When both magnets were programmed to generate magnetic flux density of 1.4 T in opposite directions with a separation

distance of 3.3 mm, the measured forces for both magnets were 103.44 N for the top magnet and -105.88 N for the bottom magnet, as can be seen in Figure 19. These values were close to the expected value of 97.5 N, which was found using Equation 1 from Section 2.2.

5.3 Hysteresis in Metal Inside a Classic C-Shaped Magnet

Due to the difficulties involved in determining the parameters needed for the Jiles Atherton method of hysteresis simulation, it was decided to employ the magnetic saturation curve method for this thesis. As such, the final basic simulation used for this project was designed to test how changing the magnetic saturation curve of a material in COMSOL would change the magnetic flux density through metal. To do this, a block of metal was placed between the poles of a classic c-shaped magnet, as shown in Figure 20.

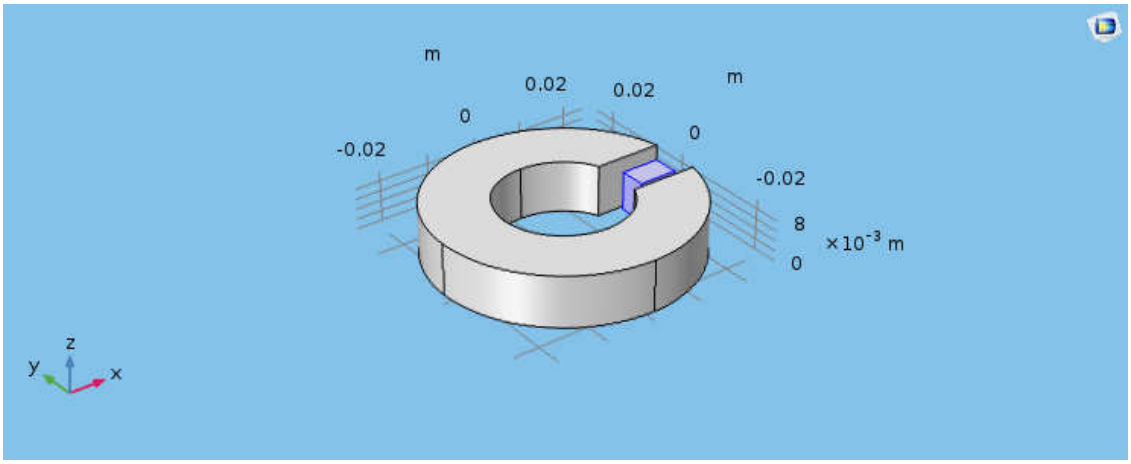

Figure 20: C-Shaped Magnet with Metal Block

Image created using COMSOL

Unlike the other basic simulations, with these tests it was not immediately clear what the numerical values of the magnetic flux should be, so instead a qualitative verification of system correctness was sought. This was achieved by altering the plot points of the BH curve and Jiles-Atherton parameters, then running simulations to check that the magnetic flux distribution varied as expected.

For the magnetic saturation method, the built-in material Soft Iron (without losses) was used. This material was tested with both the original BH curve and a modified version, both of which are given in Figure 21.

The total magnetic flux measured in the metal block was 0.98645 T with the original version and 0.98748 T with the modified version. A slight change in

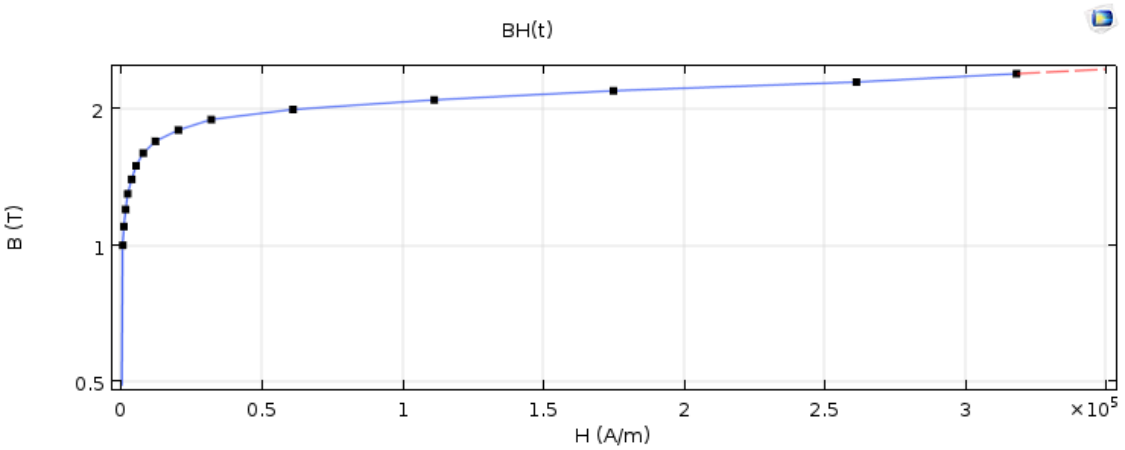

(a) Original

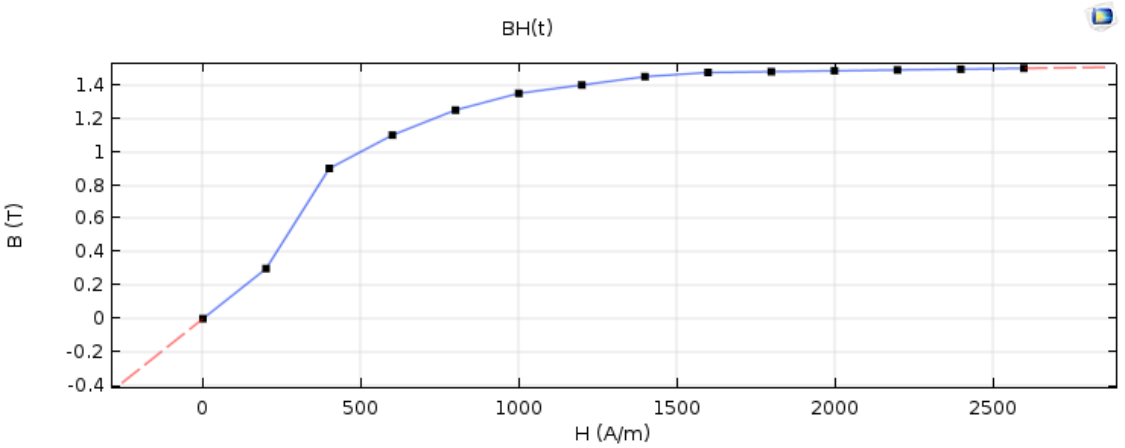

(b) Modified

Figure 21: Soft Iron (Without Losses) BH Curves

Image created using COMSOL

magnetic flux density is what was expected for the slight change in the BH curve for the iron without losses, which suggested that the magnetic saturation curve was usable for this project.

For this method, the saturation curve of the selected metal has to be imported into the software program, in this case the curve for the steel alloy SR 235, which is shown in Figure 22.

This curve was used to model hysteresis in all of the metal parts that were simulated during this thesis.

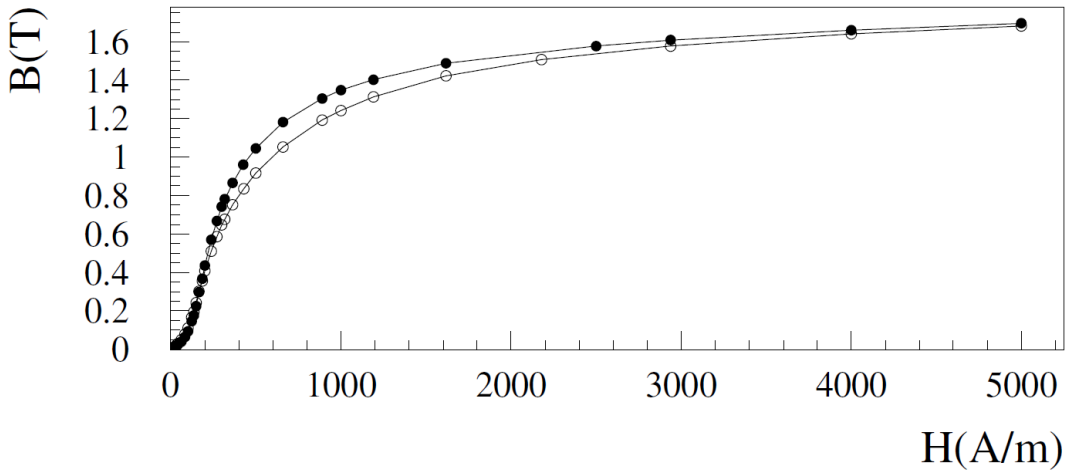

Figure 22: Magnetic Saturation Curve for SR235 (Ambrosio et al)

The solid dots show the metal used for the simulations

6 Simulations of Model 2.0

Initial simulations of Model 2.0 focused on modeling one coil glued to a circuit board and suspended between two holders, each equipped with 8 magnets with a depth of 5 mm. The geometry of this one-coil reduced system[3] can be seen in Figure 23, both with the two magnet holders visible (left) and with one magnet holder removed (right) to allow for a better view of the coil and circuit board.

In these images, the grey figures are the magnets and their holders, the orange figure is the coil, and the green is the circuit board.

Results from these simulations were compared with the measured average Lorentz force per coil found during testing with the physical system; the simulation value of 10.684 N acting on the single coil was approximately half that of the 18 ± 3 N/A per coil average value measured over the complete physical system. This difference might be explained by the small number of magnets in the reduced simulation.

When the same test was run using the larger (15 mm depth) outer magnets, a higher Lorentz force of 21.329 N was found to be acting on the coil. In this case, the small difference between this value and the 18 ± 3 N/A average measured value might be explained by the use of the larger, outer magnets instead of the

[3]although all simulations include an air sphere or cube, for simplicity this domain is often excluded from images and geometric descriptions

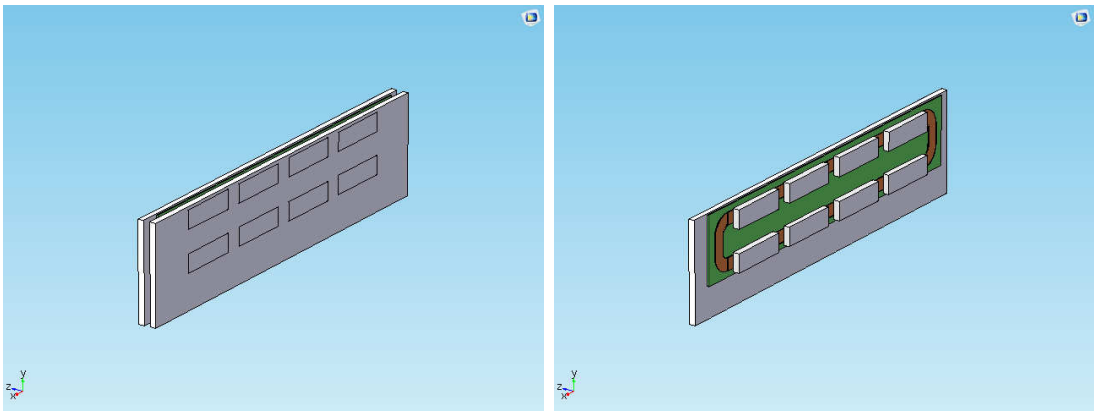

(a) With All Magnet Holders Included (b) With One Magnet Holder Removed

Figure 23: One Coil Simulation of Model 2.0

Image created using COMSOL

smaller, inner magnets that compose most of Model 2.0.

Once reasonable agreement was confirmed between the one-coil model and the real system, the entire actuator was modeled in a single simulation. A depiction of the model of the full system can be seen in Figure 24. This image shows both the complete actuator simulation (left) and a view of the actuator with several magnet holders removed (right).

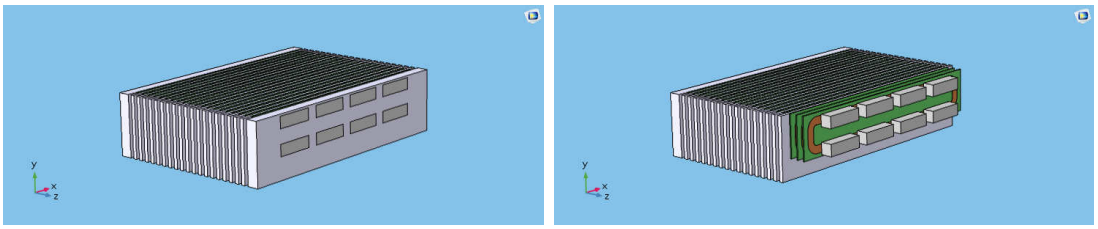

(a) With All Magnet Holders Included (b) With Some Magnet Holders Removed

Figure 24: Full System of Model 2.0

Image created using COMSOL

Modeling the entire twenty actuator system was important, as it allowed for a comparison between the values of the Lorentz force acting on coils near the actuator ends and coils near the center of the actuator. Ideally, the forces acting on the outer actuators would be slightly larger than the forces acting on the inner actuators, as larger forces would aid in starting and stopping the wave moving over the actuator surface, and this turned out to be the case, with the thicker outer magnets sufficiently augmenting the force on the outer coils to produce a force difference of 2.006 N between the outermost and innermost coils.

A graph of the force measured on each coil as a function of actuator index (with 1 being the backmost and 20 being the frontmost actuator as shown in Figure 24) is given in Figure 25.

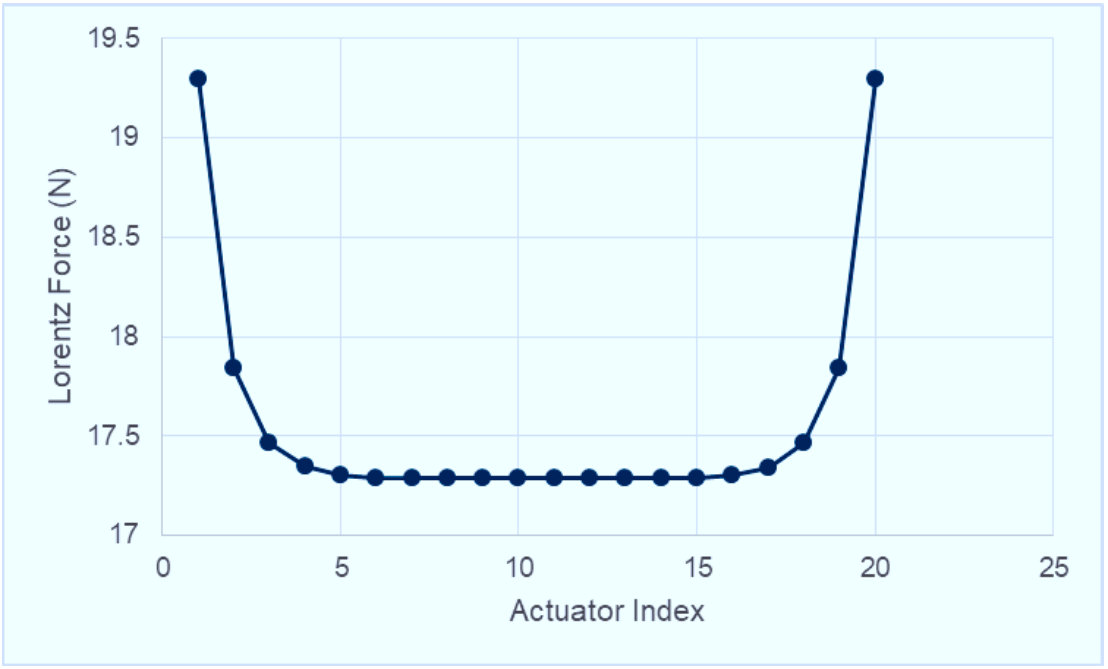

Figure 25: Lorentz Force per Ampere on Individual Model 2.0 Coils

7 Simulations of Model 3.0

After determining the pertinent values for the then-current model, Model 2.0, work began creating simulations to test different configurations to aid in the designing of Model 3.0. These new simulations involved basic tests of magnetic behavior, simulations of the intended system, and finally optimization simulations to correct for problems encountered during testing of a three-actuator prototype.

7.1 Basic Simulations in Preparation for Model 3.0

Early testing for Model 3.0 involved running simulations of two magnets of opposite polarity stacked one on top of the other, a small distance away from a second pair of stacked magnets (also with opposite polarity), as can be seen in Figure 26.

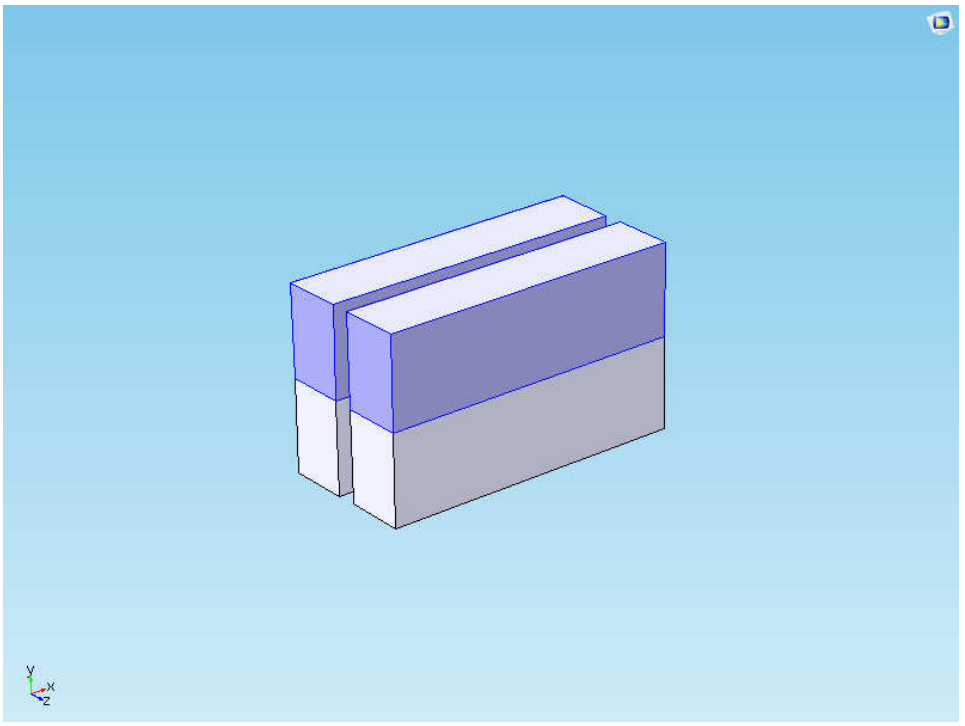

Figure 26: Two Pairs of Stacked Magnets

The top magnets (purple) are magnetized with one polarity, while the polarity of the bottom magnets (grey) is facing in the other direction

Image created using COMSOL

These simulations used magnets of a similar size[4] to those used in Model 3.0 and with the same distance between them. The tests were created because it was intended for Model 3.0 to feature magnets stacked on top of each other, and therefore it was important to verify that two magnets with different poles could touch without creating a closed loop of magnetic flux. As Figure 27 shows, in the coil location only a small zone of neutral flux was generated near the edge where the magnetic fields touched.

This small zone extended only about 2 mm, covering roughly one-fifteenth of the magnet height.

The effects of using finite element analysis are clearly visible in these images, especially the image on the right, where the tetrahedrals create strong outlines against each other. This is because the value of the magnetic flux density is only being measured at the nodes of the elements, and then extrapolated over a specific section of the tetrahedrals. Errors from these extrapolations can be reduced by reducing the size of the element mesh (thus increasing the number

[4]the height of the magnets was changed from 25 mm to 15 mm, otherwise the dimensions are identical

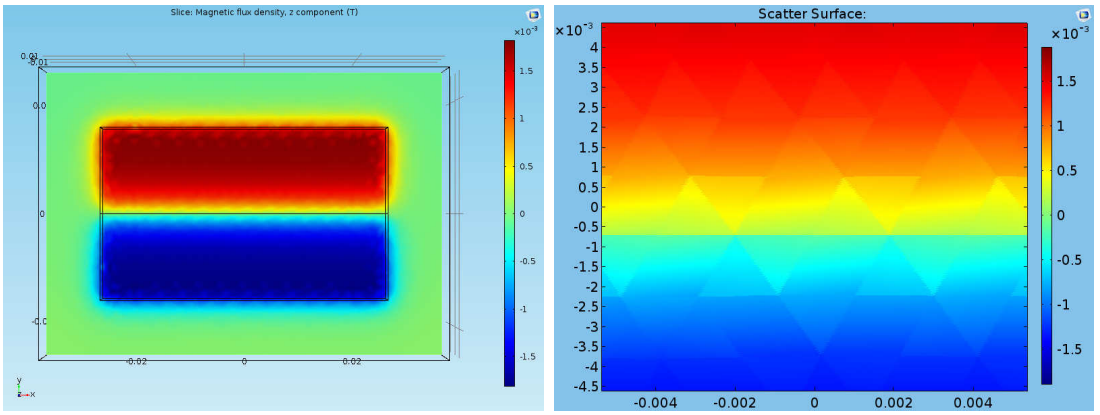

(a) Full View (b) Zoomed in on the Neutral Zone

Figure 27: Magnetic Flux Density in the Coil Location (dimensions in meters)

Image created using COMSOL

of elements and nodes), however this creates a problem - reducing the mesh too much leads to high memory use and computer overloads. As such, the mesh size was chosen to be small enough to produce a reasonable interpretation of the magnetic flux density while not overloading the computer.

Another set of simulations that were helpful in designing Model 3.0 were tests measuring the magnetic flux through the center of two pairs of stacked magnets. These tests used the same setup shown in Figure 26, and the thickness of the magnets and distance between the stacked pairs were varied. The results of these tests are presented in Figure 28.

As expected, these simulations showed that the magnetic flux density increased with increasing magnet thickness and decreasing separation distance, and were able to provide useful quantitative data as well.

7.2 Early Simulations of Model 3.0

Similarly to Model 2.0, Model 3.0 was simulated in order to compare the Lorentz force acting on the inner coils with the Lorentz force acting on the outer coils. The geometry of this simulation was composed of half of the coils and magnets from the full model, and can be seen in Figure 29.

As Figure 29 shows, this simulation still contained the full number of actuators, with each actuator containing half of the number of coils. Due to the symmetry in the system, it was possible to model only half of the device and simply double all Lorentz force values obtained with the reduced version. The Lorentz force

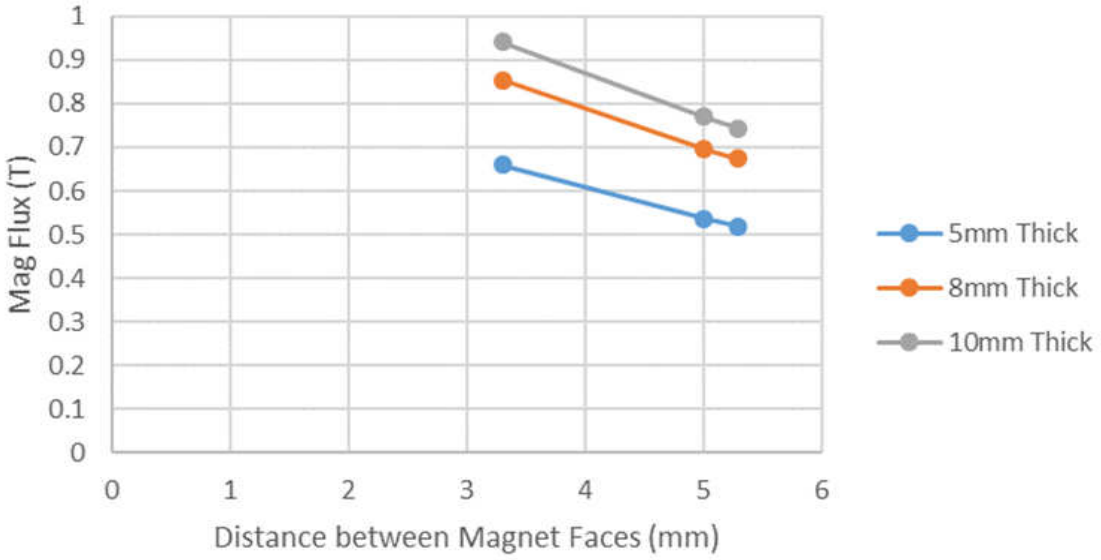

Figure 28: Magnetic Flux Density through the Gap between Magnets Pairs

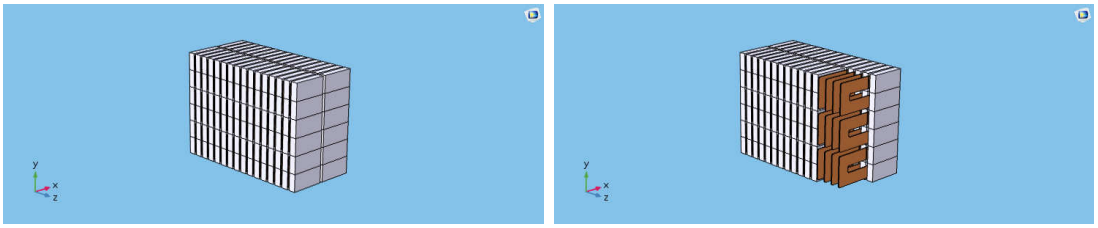

(a) Full Simulation (b) View of the Coils

Figure 29: Simulation of Model 3.0

Image created using COMSOL

per ampere for each actuator is graphed in Figure 30.

Unfortunately, unlike in Model 2.0, in Model 3.0 the inner actuators were subjected to higher Lorentz forces than the outer actuators, however, later alterations to the Model 3.0 system changed this, giving Model 3.0 a more even spread of Lorentz force values over all of the actuators. This reversal of higher and lower forces was due to all of the magnets having the same thickness, unlike in the previous model. A graph depicting the differences in Lorentz force per ampere of current for the innermost and outermost actuators of the two models is included in Figure 31.

Additionally, the forces on the coils were much higher in Model 3.0 than in Model 2.0, which can be attributed to increasing the thickness of the inner magnets, shortening the separation distance between the magnets, and changing the coil/magnet configuration so that most of the coil was embedded in a

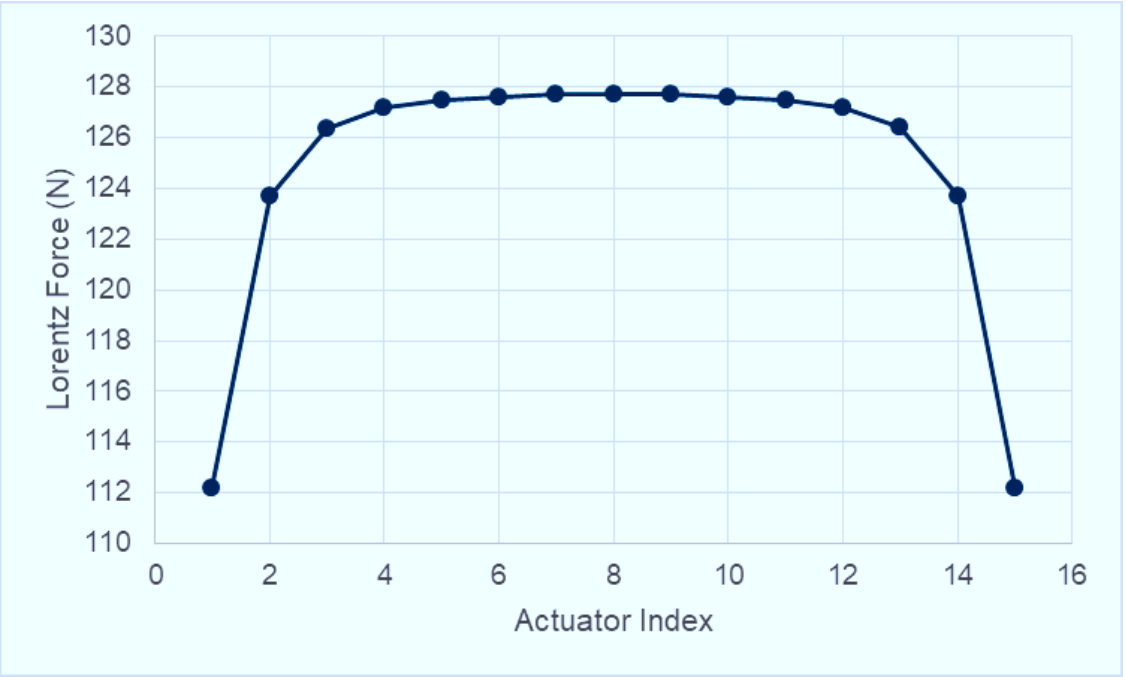

Figure 30: Lorentz Force per Ampere on Individual Model 3.0 Actuators

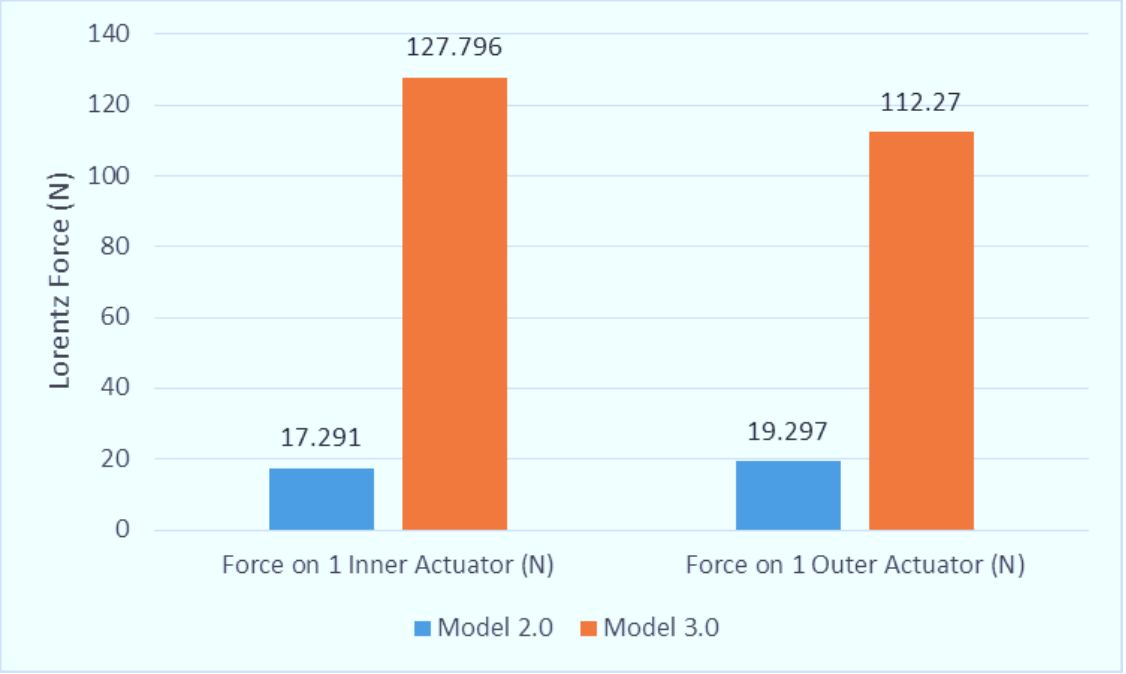

Figure 31: Lorentz Force per Ampere on Two Actuators in Models 2.0 and 3.0

field of strong magnetic flux density. A comparison of the Lorentz force distribution in the coils for the two models can be seen in Figure 32.

While for both models the Lorentz force in the y direction dropped to zero at

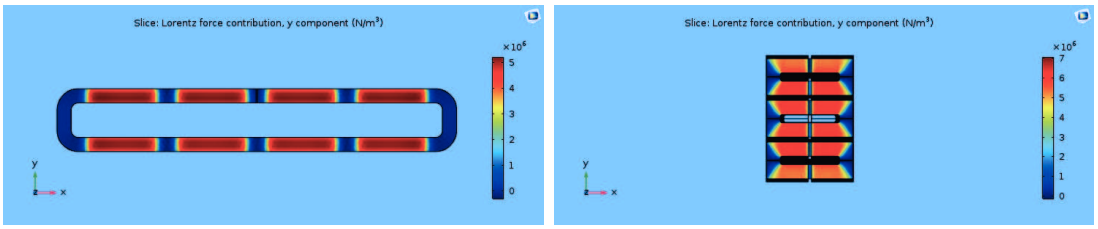

(a) Model 2.0 (full) (b) Model 3.0 (half)

Figure 32: Lorentz Force Distribution in an Actuator

Images created using COMSOL

the coil ends where the current direction changed, in Model 2.0 there were also several large gaps in Lorentz force between the magnets, as opposed to the two small gaps right in the middle of each coil in Model 3.0. Additionally, although the Model 3.0 coils were slightly smaller than the Model 2.0 coils, having multiple coils per actuator also increased the total Lorentz force.

Another consideration for Model 3.0 was the Lorentz force acting on the coils during actuation. While the model is running, the actuators move approximately 1 mm from their ideal position between the magnets. This causes a change in the amount of Lorentz force felt by the coils, and therefore affects their movement. To determine how much force the coils lose during their actuation, a parameter sweep was run over the full system, to compare the forces felt by inside and outside coils depending on their actuation position. The results of this sweep are shown in Figure 33, both for the inner and outer actuators.

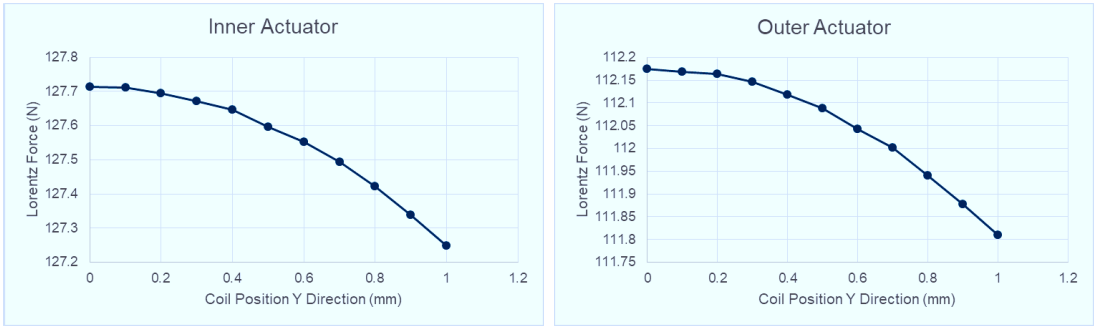

Figure 33: Lorentz Force (N) on the Coils per Ampere

0 mm shows the normal position, while 1 mm shows the fully actuated position

As the graphs in Figure 33 show, there is only an approximately 0.466 N difference in Lorentz force between the non-actuated and fully actuated position for the inner actuator , and an even smaller difference for the outer coils.

Once the parameter sweep over the coil position in the direction of the actuator motion was finished, a parameter sweep over the coil position in the direction of the magnets (z direction in the images) was begun. This sweep was intended to find the Lorentz force acting on the coils for a misaligned actuator - one that was not placed perfectly in the center of the gap between the magnets or that had been bent out of position.

Due to meshing constraints with the software[5], it was decided to run this sweep with only one actuator and two stacks of magnets, which led to a lower force on the actuator. Nevertheless, the results are still useful, as the force difference between differently positioned actuators can be compared as a percentage. The geometry of the system with a misaligned actuator is shown in Figure 34, and the results detailing the Lorentz force on the actuators is shown in Figure 35.

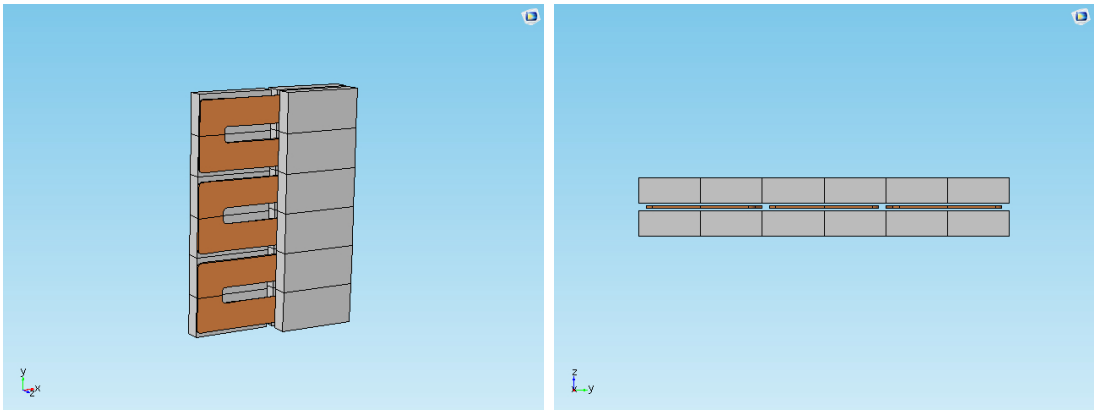

(a) Isometric View (b) Side View

Figure 34: Geometry of the Coil Position Sweep in the Z Direction Simulation

Images created using COMSOL

As Figure 35 shows, the Lorentz force on the coils is lowest around the center position, and slightly increases as the coils are moved towards the magnets, with only a 0.334 N difference in Lorentz force between the ideal and maximally misaligned positions, which is approximately 0.3 percent of the force on the ideally positioned actuator.

7.3 Optimizing Model 3.0

Following construction of a three-actuator prototype of Model 3.0, it became obvious that the full version would not work as designed. Even within the pro-

[5] an extremely fine mesh was required to simulate the small air gaps between the magnets and the coils during parts of the sweep, which in turn required a large amount of memory and long runtime

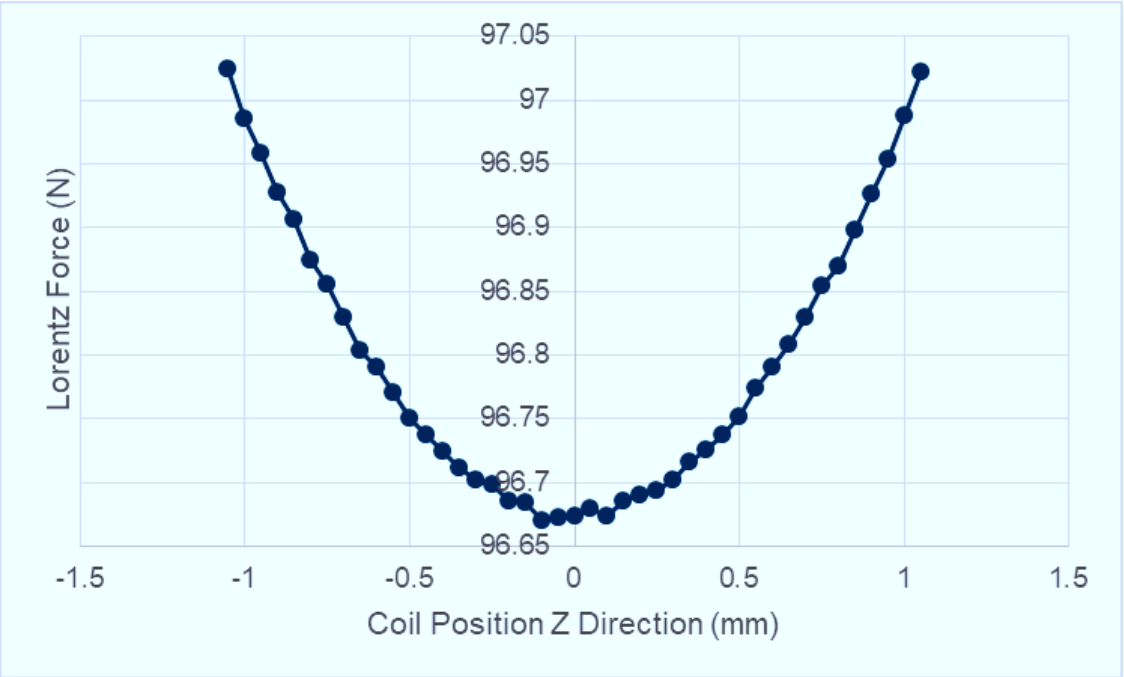

Figure 35: Lorentz Force in a One Actuator System during a Sweep of Position in the Z Direction

totype, the strong magnetic fields generated by the magnets caused several of them to be pulled from their holders. Pictures showing the after-effects of placing the magnets at their designed separation distances are shown in Figure 36.

The image on the left shows one of the magnet holders with three magnets missing and a fourth that has become dislodged, while the image on the right shows the missing three magnets attached to a different stack of magnets with one of the actuators caught in between.

In order to reduce the forces on the magnets while still maintaining a high level of magnetic flux through the actuator locations, simulations were designed which featured metal included in the system. For all of these simulations, the magnetic saturation curve method of modeling hysteresis and steel (SR235), the BH curve for which is given in Figure 22, were used.

7.3.1 Plates

The first metal configuration that was added to Model 3.0 was steel plates. These were slabs of steel with 3.3 mm thickness placed directly next to the magnets. Simulations were run with magnets of 10 mm and 5 mm thicknesses, with metal on one side and both sides of the magnets, and these were compared

Figure 36: Dislodged Magnets in the 3 Actuator Prototype

to simulations of Model 3.0 without steel plates. An example of the geometry with plates on one side of the magnets is shown in Figure 37.

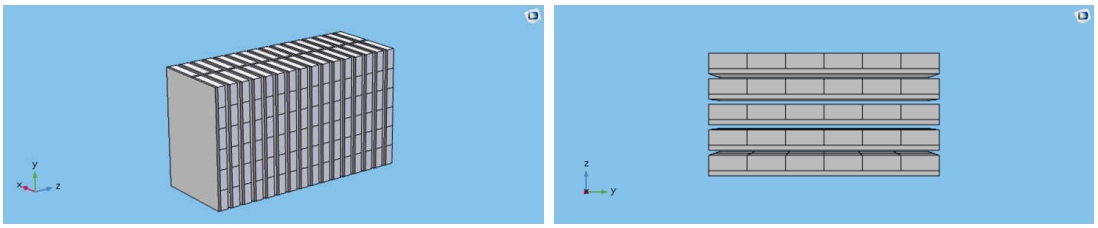

(a) Isometric View (b) Partial Side View

Figure 37: Model 3.0 with Steel Plates

Images created using COMSOL

Because the actuator is designed such that the Lorentz Force varies linearly with respect to the magnetic flux density, for these simulations the actuator coils were not included, and instead the magnetic flux was measured in each actuator location. The results of these evaluations are shown in the graph in Figure 38.

The configurations that produced the smallest amount of flux density in the actuator locations were those with steel plates placed on both sides of the mag-

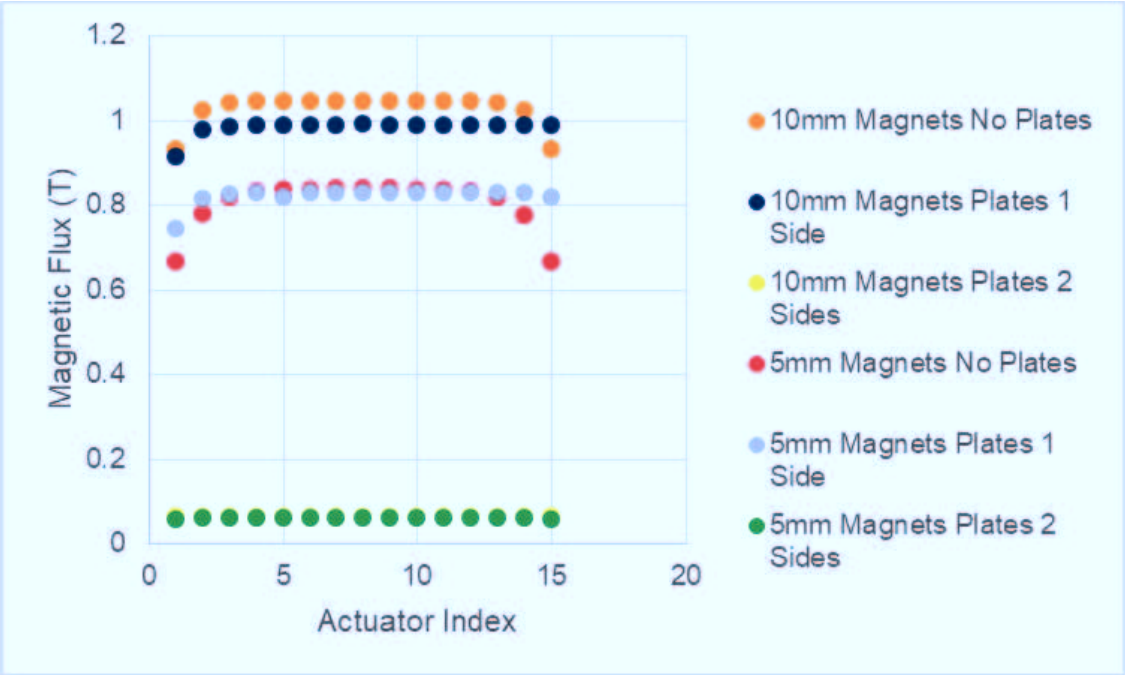

Figure 38: Magnetic Flux Through Actuator Location with Steel Plates

nets. It would seem that encasing the magnets in metal led to a kind of closing of the circuit, in which most of the flux remained in the steel and neodymium.

However, adding steel plates to one side of the magnets resulted in approximately the same amount of magnetic flux for the 5 mm magnets, and only a slight decrease in the flux density through the actuator location for the 10 mm magnets compared to the same versions without plates. As such, it was decided to continue considering steel plates on one side of the magnets in further optimization simulations.

7.3.2 U Blocks

After simulating Model 3.0 with steel plates, it was decided to simulate steel u blocks in the actuator system as well. These u blocks were made of the same material as the plates and were stacked three on top of each other, pressing against the outer magnets on both ends of the model. The geometry of a reduced system[6] with u blocks is shown in Figure 39.

[6]only nine stacks of magnets instead of sixteen

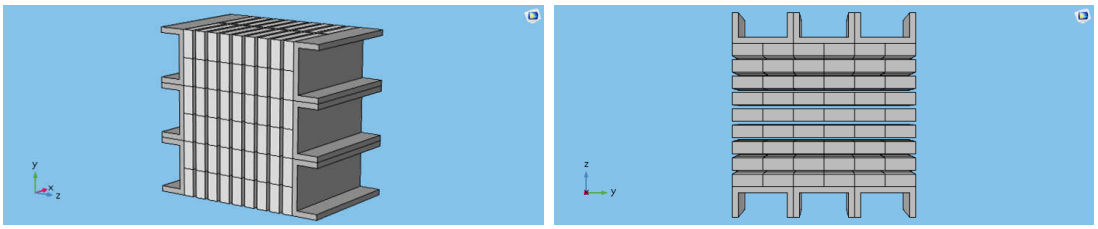

(a) Isometric View (b) Side View

Figure 39: Reduced Model 3.0 with U Blocks

Images created using COMSOL

7.3.3 Final Optimization

Simulations of the reduced, nine-stack systems were run comparing the four possible combinations of u blocks at the ends of the model and plates on one side of the magnets: without either, with only plates, with only blocks, and with both plates and blocks. These simulations were used to measure the electromagnetic forces acting on the individual magnets (all 108 per simulation) as well as the magnetic flux through the actuator location between the magnets and the Lorentz force on one of the actuators. The results of these simulations were then compared, so that the system with the best combination of low EM forces on the magnets and high Lorentz forces on the actuators could be determined.

The forces acting on the magnets were low for the inner stacks, with the highest force less than 250 N. However, the forces on the outside stacks were quite large, reaching as high as 640.75 N. In order to compare the four systems, the forces acting on one column of magnets in an outer stack were graphed for each of the four systems. Figure 40 shows the geometry of the system without plates or u blocks with an arrow pointing to the outer stack that was graphed, and Figure 41 shows the forces acting on the magnets in that stack.

As this graph shows, the highest forces were those on the system without steel plates or u blocks added, followed by the system with only u blocks, only plates, and finally the system with both plates and u blocks. In fact, the forces affecting the outside magnets in the model with both plates and blocks were comparable to the forces affecting the inner magnets - all under 250 N. Together, the plates and u blocks produced a minimum force reduction of 44 percent per magnet compared to the system without any steel, and on certain magnets that reduction was as much as 91.2 percent.

In addition to finding the electromagnetic forces on the magnets, these simulations were used to determine the magnetic flux density between the magnets. A graph showing the magnetic flux density through the actuator location in the

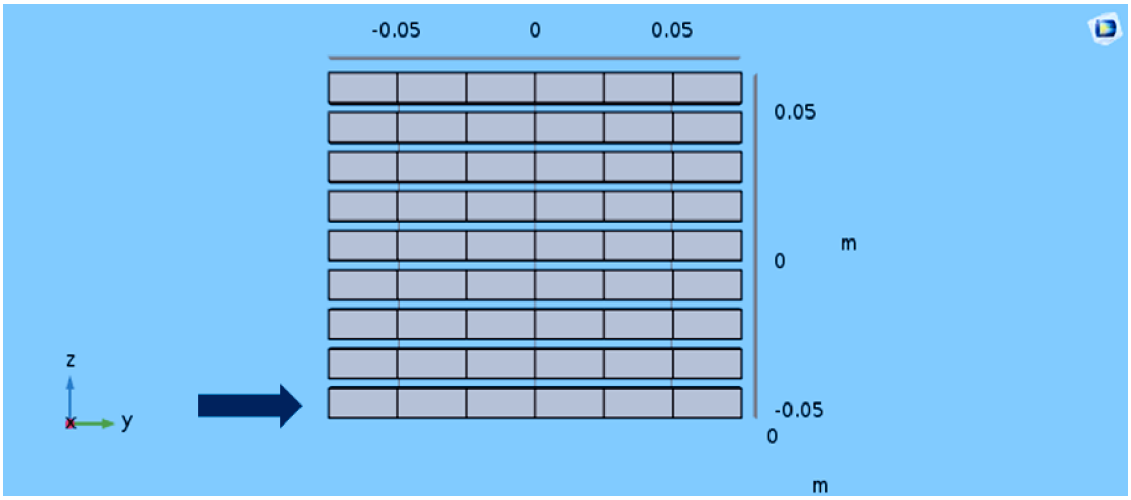

Figure 40: Arrow Pointing to the Stack of Magnets Graphed in Figure 41 for All 4 Systems

Image created using COMSOL

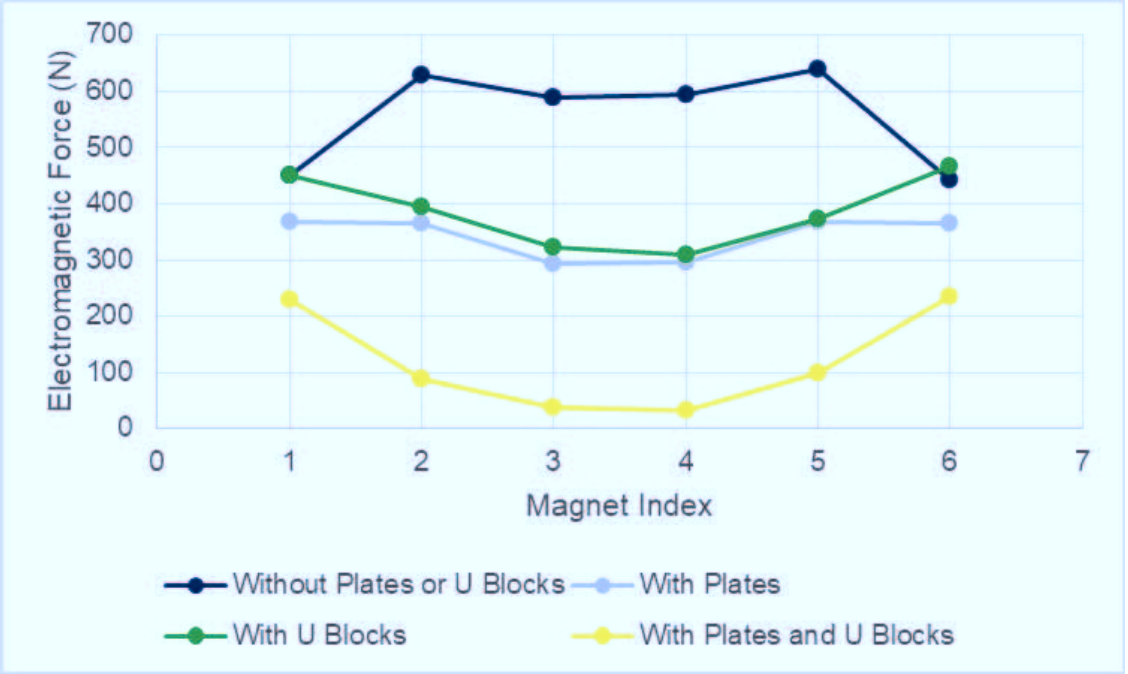

Figure 41: High EM Forces acting on the Magnets in an Outer Stack (4 Systems)

reduced systems is shown in Figure 42.

Even though the system without plates or blocks produced the highest forces on the magnets, it was the system with only blocks that produced the greatest magnetic flux through the actuator location, especially for the actuators at the ends of the model, where the magnetic flux was nearly double that of any other

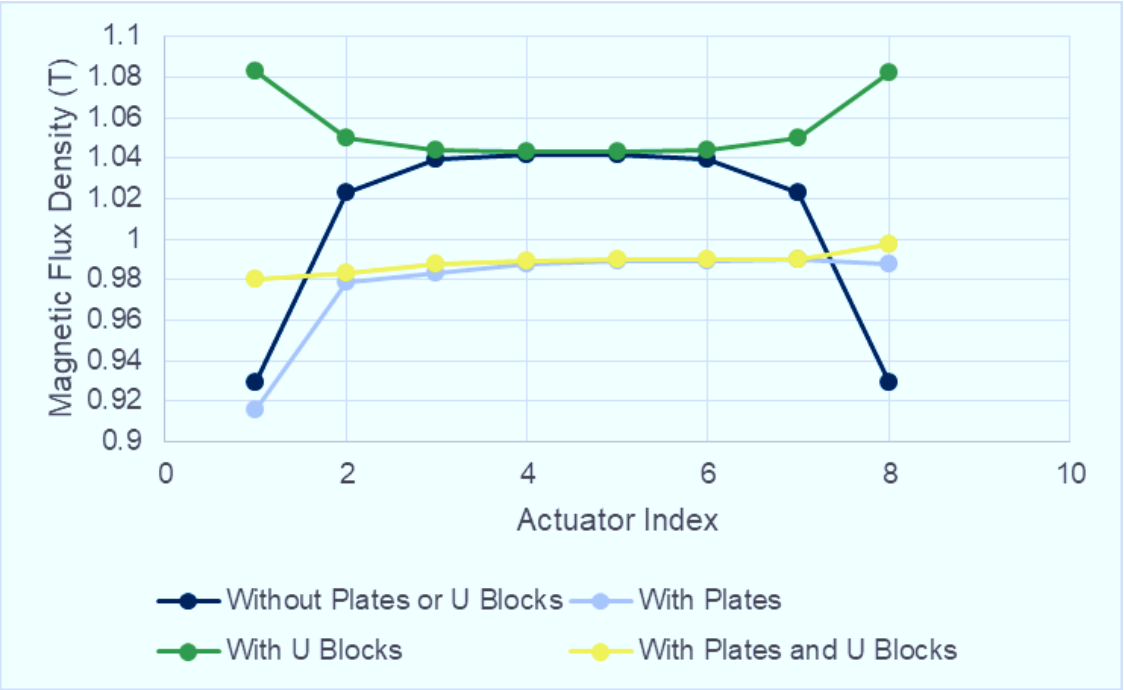

Figure 42: Magnetic Flux Density at Coil Location (4 Systems)

system simulated.

The system with the most consistency in flux density over the entire model had both plates and u blocks. This system also had a flux distribution that most closely resembled the ideal flux distribution: consistent values through actuators 2-7 and a slightly higher Lorentz force in actuator 8. Only actuator 1, with a slightly lower flux density instead of slightly higher was unideal.

Finally, these simulations were used to compare the Lorentz force in one actuator in the four systems. For this comparison, the fifth actuator, which is shown with an arrow in Figure 43, was chosen.

The results from this comparison are shown in Figure 44. As this graph shows, in actuator 5 there is only a 12.032 N difference between the system with the highest Lorentz force and the system with the lowest Lorentz force. This corresponds to only about 8 percent of the baseline system. More importantly, however, all of these values are still well within the acceptable range for meeting the actuator requirements.

Ultimately, because the system with both plates and blocks drastically lowered the EM forces on the magnets while keeping the Lorentz force within an acceptable range and producing a more desirable Lorentz force distribution over the

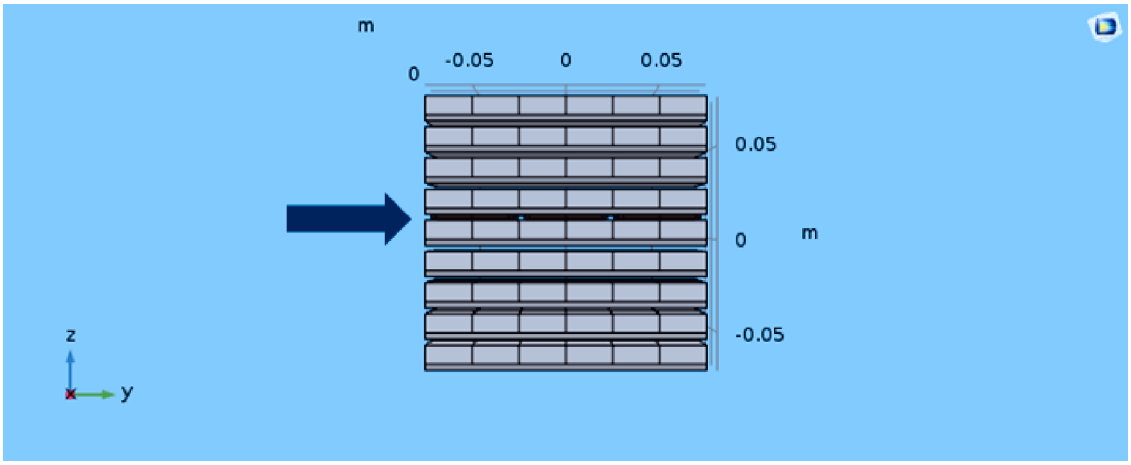

Figure 43: Lorentz Force 4 Systems Actuator Index 5

Image created using COMSOL

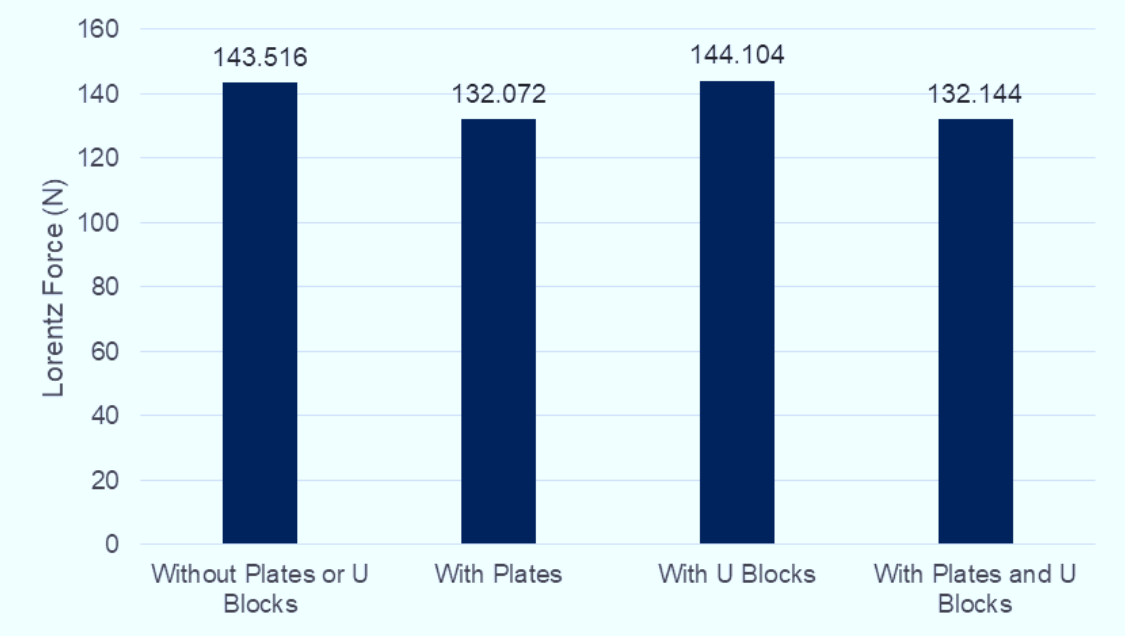

Figure 44: Lorentz Force (N) in all 6 Coils of Actuator Index 5 (4 Systems)

system, the configuration with both plates and blocks was chosen for the design of a five-actuator second prototype.

8 Conclusion and Outlook

The first two actuating systems designed for project group FOR 1779 failed to meet requirements, so a different design was needed. This Masters thesis fo-

cused on finding the optimal magnet/coil/steel configuration to produce high Lorentz force values in the actuators while at the same time producing low electromagnetic forces on the magnets. Comparisons of simulations of multiple configurations led to a choice of the final, optimum configuration, which included six coils per actuator, stacked magnets, and used steel plates and u blocks that together significantly lowered the EM forces on all of the magnets while only slightly lowering the Lorentz force on the middle actuators and actually raising the Lorentz force on the outer actuators.

Measurements taken on a three-actuator prototype showed Lorentz forces that were extremely similar to the results predicted by the simulations used in this thesis: a Lorentz force of 93 ± 5 N was measured on one of the actuators in this system, while simulations producing during this thesis predicted a force of 96.7 N for the middle actuator of the three-actuator prototype.

As of the writing of this thesis, a five-actuator prototype is in the process of being built according to the recommendations of this work. Construction on a full working Model 3.0 actuator with steel plates and u blocks should be completed near the middle of this year.

9 References

Ambrosio, M. et al. "The OPERA Magnetic Spectrometer." IEEE. 2004.

Bharat Vikas, Masanam Balakrishnan. "COMSOL Finite Element Simulation of an Electromechanical Actuator System for Turbulence Research." ZEA-2, Jülich, January 2018.

Bondeson, A.; Rylander, T.; and Ingelström, P.. "Computational Electromagnetics." New York: Springer Science+Business Media, Inc., 2005.

Clarke, R. "The Force Produced by a Magnetic Field." University of Surrey. 8 July 2010. *info.ee.surrey.ac.uk/Workshop/advice/coils/force.html*

COMSOL Inc. "AC/DC Module User's Guide." Version 5.2, 2015.

COMSOL Inc. "Company." 2018, *www.comsol.com/company.*

COMSOL Inc. "COMSOL Multiphysics User's Guide." Version 4.2, May 2012.

COMSOL Inc. "Multiphysics Cyclopedia." 2018, *www.comsol.com/multiphysics.*

DFG. GEPRIS. 12 June 2014, *http://gepris.dfg.de/gepris/projekt/202175528?language=en.*

Encyclopaedia Britannica. "Hysteresis" 2018, *https://www.britannica.com/science/hysteresis.*

Fish, Frank E. "The Myth and Reality of Gray's Paradox: Implication of Dolphin Drag Reduction for Technology." 2006 Bioinspir. Biomim.1 R17.

Griffiths, David J. "Introduction to Electrodynamics 3rd Edition" Prentice-Hall Inc, Upper Saddle River, New Jersey, September, 1999.

Harper, Douglas. Online Etymology Dictionary. 2001-2018. *www.etymonline.com*

Humphries, Stanley. "Tutorial: Theory and Applications of the Maxwell Stress Tensor." Field Precision. 2012. *www.fieldp.com/documents/stresstensor.pdf*

Klumpp, S.; Meinke, M.; and Schröder, W. "Drag reduction by spanwise transversal surface waves", Journal of Turbulence, 11:N22, 2010.

Li, W; Jessen, W.; Roggenkamp, D.; Klaas, M.; Silex, W.; Schiek, M.; and Schroeder, W. "Turbulent drag reduction by spanwise traveling ribbed surface waves." European Journal of Mechanics-B/Fluids, Vol. 53, pp. 101-112, 2015.

Lucas, Jacques et al. "Rare Earths: Science, Technology, Production and Use." Elsevier, pp. 224, 225. 9 September 2014.

Mathworks. "Inductor with Hysteresis." The MathWorks, Inc. 1994-2019. *https://www.mathworks.com/help/physmod/sps/examples/inductor-with-hysteresis.html*

Marion, Romain; Scorretti, Riccardo; Siauve, Nicolas; Raulet, Marie-Ange; Krähenbühl, Laurent. "Identification of Jiles-Atherton Model Parameters Using Particle Swarm Optimization." IEEE Transactions on Magnetics, Institute of Electrical and Electronics Engineers, 2008, 44 (6), pp. 894-897. *https://hal.archives-ouvertes.fr/hal-00287808/document*

National Physical Laboratory (NPL). "2.6.6 Magnetic Properties of Materials." 2017, *www.kayelaby.npl.co.uk*

Olsson, Magnus. "COMSOL 4.4: Magnetic Saturation Curves at your Fingertips." COMSOL Blog. 2 December 2013. *www.comsol.com/blogs/comsol-4-4-magnetic-saturation-curves/.*

Qi, Dr. H. "Jerry." "Finite Element Analysis." Colorado Boulder, Fall 2006. *www.colorado.edu/engineering/MCEN/MCEN4173/*

Rausch, Christoph. "Time-dependent Electromagnetic and Thermal Finite Element Simulation of an Actuator System for Turbulence Research." ZEA-2, Jülich, August 2018.

Takacs, Jeno. "Hysteresis Loop Reversing by Applying Langevin Approximation." Compel International Journal of Computations and Mathematics in Electrical and Electronic Engineering, July 2017.

Wen, Li; Weaver, James C.; Thornycroft, Patrick J. M.; Lauder, George V. "Hydrodynamic Function of Biomimetic Shark Skin: Effect of Denticle Pattern and Spacing." 2015 Bioinspir. Biomim. 10 066010.

List of Figures

List of Tables

Declaration of Authenticity

I hereby declare that the work presented here was formulated by myself and that no sources or tools other than those cited were used.

Bonn, 17.03.2019 _____

Jül-4422 · Oktober 2019
ISSN 0944-2952

Mitglied der Helmholtz-Gemeinschaft